Atmos. Chem. Phys. Discuss., 14, 7305–7354, 2014
www.atmos-chem-phys-discuss.net/14/7305/2014/
doi:10.5194/acpd-14-7305-2014

Atmospheric Chemistry and Physics Discussions

A global 3-D CTM evaluation of black carbon in the Tibetan Plateau

C. He[1,2], Q. B. Li[1,2], K. N. Liou[1,2], J. Zhang[3], L. Qi[1,2], Y. Mao[1,2], M. Gao[1,2], Z. Lu[4], D. G. Streets[4], Q. Zhang[5], M. M. Sarin[6], and K. Ram[7]

[1]Department of Atmospheric and Oceanic Sciences, University of California, Los Angeles, CA, USA
[2]Joint Institute for Regional Earth System Science and Engineering, University of California, Los Angeles, CA, USA
[3]Department of Atmospheric and Oceanic Sciences, School of Physics, Peking University, Beijing, China
[4]Decision and Information Sciences Division, Argonne National Laboratory, Argonne, Illinois, USA
[5]Center for Earth System Science, Tsinghua University, Beijing, China
[6]Department of Geosciences, Physical Research Laboratory, Ahmedabad, India
[7]School of Earth, Ocean and Climate Sciences, Indian Institute of Technology, Bhubaneswar, India

Received: 15 February 2014 – Accepted: 3 March 2014 – Published: 18 March 2014

Correspondence to: C. He (cenlinhe@atmos.ucla.edu)

Published by Copernicus Publications on behalf of the European Geosciences Union.

ACPD
14, 7305–7354, 2014

Abstract

We evaluate the black carbon (BC) simulations for 2006 over the Tibetan Plateau by a global 3-D chemical transport model using surface observations of BC in surface air and in snow and BC absorption aerosol optical depth (AAOD). Using updated Asian anthropogenic BC emissions (Lu et al., 2011; Zhang et al., 2009) and global biomass burning emissions (Randerson et al., 2012; van der Werf et al., 2010), model results of both surface BC and BC in snow are statistically in good agreement with observations (biases < 15 %). Model results capture the seasonal variation of surface BC concentration, but the observed wintertime high values at rural sites in the Indo-Gangetic Plain are absent in the model. Model results are in general agreement with observations (within a factor of two) at remote sites. Model simulated BC concentrations in snow are spatiotemporally consistent with observations at most sites. We find that modeled BC AAOD are significantly lower than observations to the northwest of the Plateau and along the southern slopes of the Himalayas during winter and spring, reflecting model deficiencies in emissions, topography and BC mixing state. We find that anthropogenic emissions strongly affect surface BC concentration and AAOD, while the BC aging mainly affects BC in snow over the Plateau.

1 Introduction

Black carbon (BC) is the most important light-absorbing particle formed during incomplete combustion. The major sources of BC include fossil fuel and biofuel combustion and open biomass burning (Bond et al., 2004). BC warms the atmosphere by strongly absorbing solar radiation in the visible wavelengths and in the near infrared (Ramanathan and Carmichael, 2008), influences cloud formation by acting as cloud condensation nuclei (Jacobson, 2006), and accelerates snow melting by significantly reducing snow and ice albedo (the snow albedo effect) (Flanner et al., 2007; Hansen and Nazarenko, 2004). With a total climate forcing of +1.1 $W m^{-2}$, BC is now con-

ACPD
14, 7305–7354, 2014

sidered the second most important human emission in terms of its climate forcing in the present-day atmosphere after carbon dioxide (Bond et al., 2013; Ramanathan and Carmichael, 2008). The regional warming effect of BC is even stronger, particularly over snow-covered regions (Jacobson, 2004; Flanner et al., 2007, 2009). There is evidence that BC aerosols deposited on Tibetan glaciers have been a significant contributing factor to observed rapid glacier retreat in the region (Xu et al., 2009). It has also been proposed that the radiative forcing by increasing deposition of BC in snow as an important cause for the Alps glacier retreat from last little ice age in the mid-19th century (Painter et al., 2013).

The Tibetan Plateau is the highest plateau in the world with the largest snow and ice mass outside the Polar Regions (Xu et al., 2009). The glaciers in the Plateau and the associated snowmelt are the sources of fresh water for more than one billion people in Asia (Immerzeel et al., 2010). The snowmelt from the Plateau vitally affects agriculture and hydropower through much of South, East, and Southeast Asia. The Plateau also plays a critical role in regulating the Asian hydrological cycle. Changes of snow cover affect heat flux and water exchange between the surface and the atmosphere, and further disturb the formation of the Asian monsoon (Lau and Kim, 2006).

Observations over the Tibetan Plateau show a remarkable surface temperature increase and accelerated glacier retreat in the past two to three decades (Qin et al., 2006; Prasad et al., 2009), which indicates there may be additional processes (Xu et al., 2009) besides the increasing greenhouse gases (Barnett et al., 2005). Ramanathan et al. (2005, 2007) argued that the snow melting in the Himalayas is related to the enhanced BC amount transported to this region, accounting for half of the observed warming in the region. Recent studies confirmed a strong regional warming caused by BC over the Plateau, including more than 1 % decrease of snow/ice cover (Menon et al., 2010; Lau et al., 2010), 2 ∼ 5 % reduction of snow albedo (Yasunari et al., 2010), and an increase of runoff in early spring (Qian et al., 2011). Surrounded by the world's two largest BC source regions, South Asia and East Asia (Lamarque et al., 2010), the Plateau has received an increasing BC deposition from 1951 to 2000, particularly after

ACPD
14, 7305–7354, 2014

1990 (Ming et al., 2008). Recent studies have shown that the amount of BC transported to this region has increased by 41 % from 1996 to 2010, with South Asia and East Asia accounting for 67 % and 17 % on an annual basis, respectively (Lu et al., 2012). In addition, long-range transport from Middle East, Europe, and North Africa also contributes to the BC deposition over the Plateau (Carrico et al., 2003; Kopacz et al., 2011; Lu et al., 2012).

The climate effects of BC over the Tibetan Plateau are not well understood, with large uncertainties in the estimates of BC radiative forcing (e.g. Flanner et al., 2007; Kopacz et al., 2011; Ming et al., 2013). One of the major reasons is the large discrepancy between modeled and observed BC concentrations in this region. For example, the simulations of surface BC at several Indian sites near the southern slope of the Himalayas are biased low by more than a factor of two, particularly in winter and spring, based on regional, multi-scaled and global model studies (Nair et al., 2012; Moorthy et al., 2013). Kopacz et al. (2011) and Qian et al. (2011) found significant deviations of model simulated BC in snow from observations at a number of sites over the Plateau. Sato et al. (2003) and Bond et al. (2013) pointed out large underestimates of BC absorption aerosol optical depth (AAOD) in previous models compared with Aerosol Robotic Network (AERONET) retrievals.

In this study we seek to systematically evaluate a global 3-dimentional chemical transport model (GEOS-Chem) simulation of BC in the Tibetan Plateau, against three types of surface measurements of BC : BC in surface air, BC in snow, and BC AAOD. We further delineate the effects of anthropogenic BC emissions from China and India as well as BC aging process on the simulation. Observations and model description are presented in Sect. 2. Simulations of surface BC, BC in snow and BC AAOD are discussed in Sect. 3. Sensitivity and uncertainty analyses are in Sects. 4 and 5. Finally, discussion and conclusions are given in Sect. 6.

ACPD
14, 7305–7354, 2014

2 Method

2.1 Observations

For the sake of clarity, we define here the Tibetan Plateau roughly as the region in 28° N–40° N latitudes and 75° E–105° E longitudes. We also define several sub-regions of the Plateau and adjacent regions (Fig. 1): the central Plateau (30° N–36° N, 82° E–95° E), the northwestern Plateau (36° N–40° N, 75° E–85° E), the northeastern Plateau (34° N–40° N, 95° E–105° E), the southeastern Plateau (28° N–34° N, 95° E–105° E), to the north of the Plateau (40° N–50° N, 85° E–95° E), to the northwest of the Plateau (40° N–50° N, 70° E–85° E), to the northeast of the Plateau (40° N–50° N, 95° E–105° E), and the Himalayas. There are rather limited measurements of BC in the Tibetan Plateau. Figure 1 shows sites with measurements of BC surface concentration, concentration in snow, and AAOD in the region.

2.1.1 BC surface concentration

There are 13 sites with monthly or seasonal measurements of surface BC concentration (Table 1 and Fig. 1). Observations are available for 2006 at nine of the sites. Four sites provide observations for 1999–2000, 2004–2005 or 2008–2009. We distinguish these sites as urban, rural, or remote sites based upon annual mean surface BC concentration, following Zhang et al. (2008). The concentration is typically higher than 5 $\mu g\,m^{-3}$ at urban sites (within urban centers or near strong local residential and vehicular emissions), in the range of 2–5 $\mu g\,m^{-3}$ at rural sites, and less than 2 $\mu g\,m^{-3}$ at more remote, pristine sites.

Ganguly et al. (2009b) retrieved surface BC concentration at Gandhi College site by combining aerosol optical properties from AERONET measurements and aerosol extinction profiles from Cloud-Aerosol Lidar with Orthogonal Polarization (CALIOP) observations. The retrieval is rather sensitive to errors in the aerosol single scattering albedo, size distribution and vertical profiles derived from the observations (Gan-

ACPD
14, 7305–7354, 2014

guly et al., 2009a). Measurements at Delhi (28.6° N, 77.2° E, 260 m a.s.l.), Digrugarh (27.3° N, 94.6° E, 111 m a.s.l.), Kharagpur (22.5° N, 87.5° E, 22 m a.s.l.) and Nepal Climate Observatory at Pyramid (NCOP, 28.0° N, 86.8° E, 5079 m a.s.l.) use Aethalometer (Pathak et al., 2010; Beegum et al., 2009) or Multi-angle Absorption Photometer (Nair et al., 2012; Bonasoni et al., 2010). The uncertainties of these measurements are mainly from the interference from other components in aerosols in the samples (Petzold and Schonlinner, 2004; Bond et al., 1999) and the shadowing effects under high filter loads (Weingartner et al., 2003). BC concentrations at the other sites were derived from measurements of the Thermal Optical Reflectance or Thermal Optical Transmittance (Ming et al., 2010; Ram et al., 2010a, b; Qu et al., 2008; Zhang et al., 2008; Carrico et al., 2003). The measurements are strongly influenced by the temperature selected to separate BC and organic carbon (OC) (Chow et al., 2004; Schmid et al., 2001).

2.1.2 BC concentration in snow

There are 16 sites with monthly or seasonal measurements of BC concentration in snow during 1999–2007 and two with annual measurements (Xu et al., 2006, 2009; Ming et al., 2009a, b, 2012, 2013). These sites are at high-elevation (> 3500 m a.s.l.), remote locations in the Himalayas and other parts of the Plateau (Table 2 and Fig. 1). The snow and ice samples taken from these sites are heated and filtered through fiber filters in the laboratory. Thermal techniques (Cachier and Pertuisot, 1994; Chow et al., 2004) are then used to isolate BC from other constituents (especially OC) in the filters, followed by analysis using carbon analyzers including heating-gas chromatography (Xu et al., 2006), optical carbon analysis (Chow et al., 2004) and coulometric titration-based analysis (Cachier and Pertuisot, 1994). The accuracy of the heating-gas chromatography system is dominated by the variability of the blank loads of pre-cleaned filters (Xu et al., 2006). The coulometric titration-based analysis measures the acidification of the solution by carbon dioxide produced from BC combustion in the system (Ming et al., 2009a), where the pH value of the solution may be interfered by other ions.

ACPD
14, 7305–7354, 2014

2.1.3 AERONET AAOD

There are 14 AERONET sites with AAOD retrievals in the Tibetan Plateau and adjacent regions (Table 3 and Fig. 1). These sites are mostly in the Indo-Gangetic Plain, in northern India and along the southern slope of the Himalayas. We infer BC AAOD from monthly averaged AOD data from 2006 to 2012, following Bond et al. (2013). The measurements provide sun and sky radiance observations in the mid-visible range (Dubovik and King, 2000), which allows for inference of aerosol column absorption from retrievals of AOD and single scattering albedo (SSA) via AAOD = AOD × (1 − SSA). Both BC aerosols and dust particles contribute to the absorption. The absorption by fine-mode aerosols is primarily from BC while the absorption by larger particles (diameter > 1 µm) is principally from dust. Dust AAOD is estimated from the super-micron part of aerosol size distributions provided by the AERONET retrieval method and an assumed refractive index of 1.55 + 0.0015i (Bond et al., 2013). BC AAOD is then the difference between the total and dust AAOD. This process attributes all fine-mode aerosol absorption to BC. Because of the contributions from OC and fine dust particles to fine-mode AAOD, the inferred BC AAOD is likely biased high. Bond et al. (2013) estimated that the uncertainty from the impacts of dust and OC on the fine-mode AAOD can be as large as 40–50 %. The limited AERONET sampling in this region is another source of uncertainty (Bond et al., 2013).

2.2 Model description and simulations

The GEOS-Chem model is driven by assimilated meteorology from the Goddard Earth Observing System (GEOS) of the NASA Global Modeling and Assimilation Office (GMAO). We use here GEOS-Chem version 9-01-03 (available at http://geos-chem.org), driven by GEOS-5 meteorological fields. The meteorological fields have a native horizontal resolution of 0.5° × 0.667°, 72 vertical layers, and a temporal resolution of 6 h (3 h for surface variables and mixing depths). The spatial resolution is degraded to 2° × 2.5° in the horizontal and 47 layers in the vertical (from the surface to 0.01 hPa) for

ACPD
14, 7305–7354, 2014

computational expediency. The lowest model levels are centered at approximately 60, 200, 300, 450, 600, 700, 850, 1000, 1150, 1300, 1450, 1600, 1800 m a.s.l.

Tracer advection is computed every 15 min with a flux-form semi-Lagrangian method (Lin and Rood, 1996). Tracer moist convection is computed using GEOS convective, entrainment, and detrainment mass fluxes as described by Allen et al. (1996a, b). The deep convection in GEOS-5 is parameterized using the relaxed Arakawa–Schubert scheme (Moorthi and Suarez, 1992; Arakawa and Schubert, 1974), and the shallow convection treatment follows Hack (1994). Park et al. (2003, 2006) first described GEOS-Chem simulation of carbonaceous aerosols.

2.2.1 BC emissions

The global anthropogenic BC emissions are from Bond et al. (2007), with an annual emission of 4.4 Tg C for the year 2000. Anthropogenic BC emissions in Asia, chiefly in China and India, have increased significantly since 2000 (Granier et al., 2011). Zhang et al. (2009) developed an Asian anthropogenic BC emissions (for China and India and the rest of Asia) for 2006 for the Intercontinental Chemical Transport Experiment-B (INTEX-B) field campaign (Singh et al., 2009), with considerable updates to a previous inventory developed by Streets et al. (2003). They employed a dynamic methodology that accounts for rapid technology renewal and updated the fuel consumption data. Lu et al. (2011) further updated the activity rates, technology penetration data and emission factors in China and India, and reported anthropogenic BC emissions only in these two countries for 1996–2010. Table 4 is a summary of the two inventories. Anthropogenic BC emissions in India are lower in the Zhang et al. (2009) inventory (hereinafter the INTEX-B inventory) than in the Lu et al. (2011) inventory (hereinafter the LU inventory) by a factor of two, while emissions in China are 10 % higher in the INTEX-B inventory than in the LU inventory (Table 4). The higher emissions in India in the LU inventory are primarily a result of the updated biofuel emission factors and the new method used to estimate biofuel consumptions. The biofuel emissions, which are dominated by residential burning, account for more than 50 % of total BC emissions in

ACPD
14, 7305–7354, 2014

India (Lu et al., 2011). There are large uncertainties in both inventories. The uncertainty in the LU inventory ranges from −43 % to 93 % for China and from −41 % to 87 % for India (Lu et al., 2011), while it is ±208 % for China and ±360 % for India in the INTEX-B inventory (Zhang et al., 2009).

Global biomass burning emissions are from the Global Fire Emissions Database version 3 (GFEDv3) (van der Werf et al., 2010). Kaiser et al. (2012) showed that GFEDv3 underestimates carbon emissions by a factor of 2–4 globally because of undetected small fires. Randerson et al. (2012) reported an updated GFEDv3 inventory that accounts for small fire emissions. Small fires increase carbon emissions by 50 % in Southeast Asia and Equatorial Asia (Randerson et al., 2012). We use the GFEDv3 emissions with a monthly temporal resolution in the present study. The uncertainty of the GFEDv3 emissions is at least 20 % globally and higher in boreal regions and Equatorial Asia (van der Werf et al., 2010). The major uncertainty lies in insufficient data on burned area, fuel load and emission factor (van der Werf et al., 2010; Randerson et al., 2012).

2.2.2 BC deposition

Simulation of aerosol dry and wet deposition follows Liu et al. (2001). Dry deposition of aerosols uses a resistance-in-series model (Walcek et al., 1986) dependent on local surface type and meteorological conditions. There have since been many updates. A standard resistance-in-series scheme (Wesely, 1989) has been implemented in the non-snow/non-ice regions (Wang et al., 1998) with a constant aerosol dry deposition velocity of 0.03 $cm\,s^{-1}$ prescribed over snow and ice (Wang et al., 2011). This velocity is within the range (0.01–0.07 $cm\,s^{-1}$) employed in Liu et al. (2011) to improve the BC simulation in the AM3 global model (Donner et al., 2011). We found that dry deposition accounts for 20 % of the total BC deposition over the Tibetan Plateau in winter and 10 % in summer.

Liu et al. (2001) described the wet scavenging scheme for aerosols in the GEOS-Chem. Wang et al. (2011) implemented in the model a new below-cloud scavenging

ACPD
14, 7305–7354, 2014

parameterization for individual aerosol mode, which distinguishes between the removal by snow and by rain drops for aerosol washout. They also applied different in-cloud scavenging schemes to cold and to warm clouds, and with an improved areal fraction of a model grid box that experiences precipitation. These changes are included in the GEOS-Chem version used for the present study.

The GEOS-Chem model does not directly predict BC (or any aerosols for that matter) in snow at the surface in the absence of a land-surface model that explicitly treats snow including its aging. As an approximation, we estimate BC concentration in snow in the model as the ratio of total BC deposition to total precipitation, following Kopacz et al. (2011) and Wang et al. (2011). The use of total precipitation here is justified considering the low temperature typically over the Tibetan Plateau (Wu and Liu, 2004). We also neglect the aging of surface snow, which potentially can be important. Our calculation of BC concentration in snow assumes a well mixing of BC and snow. However, BC content is not uniform throughout a snow column. Thus, an ideal comparison of modeled and observed BC concentration in snow should be for the same depth of a snow column. Also, ignoring snow aging and internal mixing of snow and BC conceivably contributes to the underestimate of BC concentration in snow in the model. This may be an especially important issue for comparisons in the central Plateau and to the north of the Plateau, where snow melting has been suggested to strongly increase BC concentration in snow (Zhou et al., 2007; Ming et al., 2013).

2.3 BC aging

Freshly emitted BC is mostly (80 %) hydrophobic (Cooke et al., 1999). Hydrophobic BC becomes hydrophilic typically on the timescale of a few days (McMeeking et al., 2011 and references therein), because of coating with soluble materials like sulfate and organic matter (Friedman et al., 2009; Khalizov et al., 2009). The internal mixing of BC and other aerosol constituents significantly changes the morphology, hygroscopicity and optical properties of BC particles (Zhang et al., 2008). This further influences BC absorption efficiency (Bond et al., 2006) and lifetime against deposition (Mikhailov

ACPD
14, 7305–7354, 2014

et al., 2001). However, the aging process is not explicitly simulated in the GEOS-Chem, where an e-folding time of 1.15 days for the conversion of hydrophobic to hydrophilic BC is simply assumed (Park et al., 2005; Kopacz et al., 2011; Wang et al., 2011). Liu et al. (2011) proposed a parameterization for BC aging where the conversion time is not uniform but varies. Specifically, the conversion is assumed to be primarily a result of sulfuric acid deposition (condensation) onto BC particles and the mass deposition rate is proportional to the concentration of gaseous sulfuric acid and to the BC particle surface area. Gaseous atmospheric sulfuric acid is a product of sulfur dioxide oxidation by the hydroxyl radical (OH). Consequently its steady-state concentration is linearly linked to OH concentration. Thus, in the absence of nucleation and coagulation, the BC aging rate can be parameterized as a linear function of OH concentration.

2.4 Simulations

For the present study, we conducted three GEOS-Chem simulations for 2006 (Table 5). Detailed discussions and justifications for these model experiments are provided below where appropriate. Model results are sampled at the corresponding locations of the measurement sites. Model results presented here are monthly averages. As pointed out in previous studies (Mao et al., 2011; Fairlie et al., 2007), comparing localized observations with model results that are representative of a much larger area is inherently problematic. The mountainous sites and the complex terrain in the Tibetan Plateau further complicate the comparison.

In experiment A, we replace the Bond et al. (2007) emissions in China and India with the LU inventory and use the INTEX-B inventory for the rest of Asia. This is our standard simulation and the results are used for all model evaluations presented here unless stated otherwise. We find that wet deposition accounts for 83 % of the global annual BC deposition, consistent with the previous results of 78.6 ± 17 % from the Aerosol inter-Comparison project (AeroCom) multi-model study (Textor et al., 2006). The tropospheric lifetime of BC against deposition is 5.5 days, within the range of 5–11 days reported by Koch et al. (2009). The difference between experiments B and A is that we

ACPD
14, 7305–7354, 2014

replace the Bond et al. (2007) emissions in China and India with the INTEX-B inventory in experiment B. By contrasting model results from these two experiments, we aim to assess the sensitivity of BC in the Tibetan Plateau to changes in the anthropogenic emissions from India and China, the two largest source regions of BC to the Plateau (Kopacz et al., 2011), as will be discussed in further details in Sect. 4. Both experiments A and B use an e-folding time of 1.15 days for BC aging. Experiment C applies the Liu et al. (2011) parameterization for BC aging instead. We used monthly mean OH concentrations with diurnal variations in the parameterization, which is derived from the offline GEOS-chem simulation with the same spatial resolution as BC simulations. The resulting e-folding time is 2.5 days on average globally and 2 days in Asia. The longer e-folding time results in longer atmospheric lifetime, larger deposition and higher hydrophobic fraction of BC over the Tibetan Plateau (not shown). We discuss further in Sect. 5 the differing results between experiments C and A, which allow us to appraise the effect of a variable BC aging time on BC in the Plateau.

3 Results

3.1 BC in surface air

Surface concentrations of BC at Lhasa and Delhi, two urban sites (see Table 1), are strongly affected by emissions from city traffic and industries (Zhang et al., 2008; Beegum et al., 2009). The BC concentrations at Dibragarh are highly impacted by the emissions from the oil wells upwind and vehicular emissions from national highways nearby (Pathak et al., 2010). The concentrations at Dunhuang, a well-known tourist attraction and archaeological site, likely reflect vehicular emissions associated with tourist traffic including tour buses. All four sites are characterized by strong local emissions. Model results reproduce the seasonal trends at these "urban" sites (sites that are near urban centers or heavily influenced by local emissions), but are low by

ACPD
14, 7305–7354, 2014

an order of magnitude (Fig. 2 and Table 1). We thus exclude these four sites from our analysis hereinafter.

Figure 3 shows surface BC concentrations at Kharagpur (22.5° N, 87.5° E, 28 m a.s.l., Fig. 3a), Gandhi College (25.9° N, 84.1° E, 158 m a.s.l., Fig. 3b) and Kanpur (26.4° N, 80.3° E, 142 m a.s.l., Fig. 3c), three rural sites. Model results reproduce the observed BC concentrations with the exception of winter, when the model underestimates the concentrations by 50 %. The high wintertime concentrations are primarily because of emissions from agricultural waste and wood fuel burning that is dominant over the Indo-Gangetic Plain during winter (Ram et al., 2010b). The wintertime low biases in the model therefore clearly call for improved (increased) emission estimates. Moorthy et al. (2013) found that modeled surface BC concentrations in this region are underestimated by more than a factor of two during winter when the planetary boundary layer (PBL) is convectively stable, while model underestimates are smaller in summer when the PBL is unstable. They suggested that the overestimate of wintertime PBL height in chemical transport models is an important contributor to model underestimates of surface pollutant concentrations. Lin and McElory (2010) pointed out that the assumption of full PBL mixing (instantaneous vertical mixing throughout the mixing depth) in the GEOS-Chem tends to overestimate vertical mixing under a stable PBL condition. They proposed and implemented in GEOS-Chem a non-local PBL mixing scheme (Holtslag and Boville, 1993; Lin et al., 2008), where the mixing states are determined by static instability. They used a local K-theory scheme (Louis, 1979) for a stable PBL and added a "non-local" term for an unstable PBL to account for the PBL-wide mixing triggered by large eddies. Our results show that the non-local boundary layer mixing increases surface BC concentrations by up to 25 % in winter and spring, a significant improvement. Nair et al. (2012) showed that the non-local boundary layer mixing still tends to overestimate the vertical mixing during winter in the Indo-Gangetic Plain.

Model results are within ±50 % of the observations at two remote sites, Zhuzhang (28.0° N, 99.7° E, 3583 m a.s.l., Fig. 3h) and NCOS (30.8° N, 91.0° E, 4730 m a.s.l., Fig. 3i), where observations are available for only fall and winter. Model results are

ACPD
14, 7305–7354, 2014

lower than the observations at NCOP (28.0° N, 86.8° E, 5079 m a.s.l., Fig. 3e) and Nagarkot (27.7° N, 85.5° E, 2150 m a.s.l., Fig. 3g) by a factor of two in spring. The latter two sites are influenced by emissions from nearby Nepal valleys transported by the mountain-valley wind (Carrico et al., 2003; Bonasoni et al., 2010). In contrast, model results capture the relatively high concentrations in winter and spring observed at Manora Peak (29.4°,79.5° E,1950 m a.s.l., Fig. 3d) and Langtang (28.1° N, 85.6° E, 3920 m a.s.l., Fig. 3f), but overestimate the summertime concentrations by a factor of two. Part of the discrepancies is explained by the inherent difficulty in simulating the meteorological fields over the complex Himalayan terrain. Chen et al. (2009) showed that the terrain effects and meteorological features in the Tibetan Plateau are not entirely reproduced by the GEOS-5 meteorological fields. Such difficulty is not unique to the Himalaya region. Emery et al. (2012) also showed that the transport of chemical species is not well simulated over the complex terrain in the western US using GEOS-Chem with GEOS-5 meteorological fields 2° × 2.5°.

There is a small negative bias of $-0.3\,\mu g\,m^{-3}$ in model simulated surface BC concentrations (Fig. 4, left column), and the difference between model results and the observations is statistically insignificant. Overall, the model reproduces the spatiotemporal variation of surface BC concentrations in the Tibetan Plateau (r = 0.9, root-mean-square-error RMSE = $1.3\,\mu g\,m^{-3}$), but misses the high values (Fig. 4).

3.2 BC in snow

BC deposition and precipitation together determine BC concentration in snow, which we approximate as the ratio of total BC deposition to total precipitation (see Sect. 2.2.2). Figure 5 shows GEOS-Chem simulated annual mean BC deposition and GEOS-5 precipitation over Asia. The largest depositions over the Tibetan Plateau are in the Himalayas and the southeastern Plateau (Fig. 5a), reflecting the proximity of strong BC sources in northern India and southwestern China (Lu et al., 2012) and the intense precipitation in the region (Fig. 5b). The northern Plateau is heavily influenced by BC

ACPD
14, 7305–7354, 2014

transported in the westerlies (Kopacz et al., 2011; Lu et al., 2012), but the lack of strong precipitation (Fig. 5b) results in considerably small BC deposition (Fig. 5a).

Table 2 shows BC concentrations in snow at 18 sites across the Plateau. The concentrations are 30 % lower during the monsoon season (June–September) than during the non-monsoon seasons (October–May), both in the observations and in the model. Here the monsoon and non-monsoon seasons are defined following Xu et al. (2009). The lowest concentrations (minimum of 4.3 $\mu g\,kg^{-1}$) are seen in the northern slope of the Himalayas, while the highest values (maximum of 141 $\mu g\,kg^{-1}$) are found to the north of the Plateau. Such spatial variation largely reflects the different elevations of the sites. Ming et al. (2009a, 2013) have shown that observed BC concentration in snow over the Tibetan Plateau is inversely correlated with the elevation of a site, with lower concentrations at higher elevations. Our model results capture this spatial variation, but deviate from the observations by more than a factor of two at several sites in the Himalayas and the central Plateau (Table 2).

Model results overestimate BC concentrations in snow during the monsoon by a factor of 2–4 at three Himalayan sites, Zuoqiupu (29.2° N, 96.9° E, 5500 m a.s.l.), East Rongbuk (28.0° N, 87.0° E, 6500 m a.s.l.) and Namunani (30.4° N, 81.3° E, 5900 m a.s.l.) (Fig. 6). Wet scavenging accounts for more than 80 % of the BC deposition over the Tibetan Plateau during the monsoon season in the model. The large overestimate in the model implies either excessive wet deposition or too weak precipitation or both in the Himalayas, given that BC concentration in snow is approximated as the ratio of BC deposition to total precipitation (see Sect. 2.2.2). Figure 7 shows the monthly precipitation over different parts of the Tibetan Plateau from the Global Precipitation Climatology Project (GPCP, Huffman et al., 2001), the NOAA Climate Prediction Center (CPC) Merged Analysis of Precipitation (CMAP, Xie and Arkin, 1997), the University of East Anglia Climate Research Unit (CRU, Harris et al., 2014) and GEOS-5. GPCP precipitation is generally consistent with that from CMAP in most parts of the Plateau except the southeastern Plateau, where it is stronger by more than a factor of two. CRU precipitation tends to be much stronger than those from GPCP and CMAP during the monsoon

ACPD
14, 7305–7354, 2014

season, particularly in the southeastern Plateau and the Himalayas (Fig. 7). Previous studies have shown that the monsoon precipitation in the Himalayas is too weak in both GPCP and CMAP data (Kitoh and Kusunoki, 2008; Voisin et al., 2008) yet too strong in the CRU data (Zhao and Fu, 2006; Xie et al., 2007). The scarcity of observational sites and the complex terrain of the Himalayas are two of the principle reasons for large uncertainties in and apparent inconsistences among different precipitation datasets (Ma et al., 2009; Andermann et al., 2011). Figure 7 shows that GEOS-5 precipitation is stronger than GPCP and CMAP data by a factor of two in the Himalayas during the monsoon season. To probe the sensitivity of BC deposition and our calculated BC concentration in snow in the Himalayas to precipitation, we conducted a GEOS-Chem simulation where we reduced GEOS-5 precipitation in the region by 20 % during the monsoon season. The resulting BC wet deposition is only slightly lower (up to 5 %), rather insensitive to changes in presumably already intense precipitation during the monsoon season in the region. This lack of strong sensitivity reflects an already efficient wet scavenging of BC in the intense monsoon precipitation. The resulting BC concentrations in snow are higher by 18 % on average in the region, because the reduced precipitation tends to concentrate BC in snow. Therefore, model overestimates of BC concentration in snow in the region cannot be resulted from the overestimate of monsoon precipitation but from the excessive BC deposition. This is likely a result of overlong BC lifetime due to insufficient wet removal. Wang et al. (2014) compared GEOS-Chem simulated atmospheric BC concentrations with the HIAPER Pole-to-Pole Observations (HIPPO) aircraft measurements and concluded that wet scavenging in the model is too weak. The excessive deposition is also likely because of too strong PBL mixing, which lifts up excessive BC into the free troposphere. Our results show that the non-local boundary layer mixing (Lin and McElory, 2010) reduces BC wet deposition by up to only 5 % on average in the Himalayas during the monsoon season.

Figure 6 shows that our calculated BC concentrations in snow are lower than observations by a factor of two across the sites in the central Plateau. Ming et al. (2009a) pointed out that this region is predominantly influenced by biofuel burning (residential

ACPD
14, 7305–7354, 2014

cooking and heating) and biomass burning from religious activities. These local emissions are largely unaccounted for in current emission inventories (Wang et al., 2012). In addition, it is likely that the lack of consideration of snow aging leads to lower estimate of BC concentration in snow (Xu et al., 2006). We do not include two sites, Meikuang and Zhadang, in the comparison here, because of local emissions from coal-containing rock strata (Xu et al., 2006) at the former and strong snow melting (Zhou et al., 2007) at the latter. GEOS-5 precipitation in the central Plateau is in general agreement with those from CMAP and CRU during the non-monsoon season and that from GPCP during the monsoon season (Fig. 7e).

Model results are consistent with observations at the elevated sites in the northwestern and northeastern Plateau and to the north of the Plateau (Fig. 6), where free tropospheric BC is dominated by northern mid-latitude pollution transported by the westerlies (Kopacz et al., 2011; Lu et al., 2012). Regional emissions from western and central China also contribute to BC deposition in these regions (Lu et al., 2012). Although precipitation in these regions is weaker in GEOS-5 than in GPCP and CMAP (Fig. 7b and d), previous studies have shown that GPCP and CMAP precipitation is likely too strong there (Voisin et al., 2008; Ma et al., 2009).

Overall model results of BC concentration in snow have a small negative bias but a large RMSE (Fig. 4, middle column) caused by the large discrepancies in the Himalayas and the central Plateau. Model results are statistically in good agreement with observations and reproduce the observed spatiotemporal variation (r = 0.85).

3.3 BC AAOD

Modeled BC AAOD is consistently biased lower than the AERONET retrievals at most sites on both a monthly (Fig. 4, right column) and an annual basis (Table 3). The annual mean modeled BC AAOD over the Tibetan Plateau is 0.002 (Fig. 8), considerably lower than the observations. Model results somewhat capture the observed spatial and seasonal trends (r = 0.53), but to varying degrees underestimate the magnitudes (Fig. 9). Forty percent of the data points are too low by more than a factor of two in the

ACPD
14, 7305–7354, 2014

model, particularly at sites in the Himalayas and to the northwest of the Plateau, especially during the large emission seasons of winter and spring. Most of the AERONET measurements in and around the Plateau are from after 2006, while our model results are for only 2006. BC emissions in India have increased by 3.3 % yr^{-1} since 2006 (Lu et al., 2011). Therefore the large low bias of model results clearly bears out the abovementioned temporal (hence emission) match. We also note that there are large uncertainties in the AERONET AAOD retrieval (Bond et al., 2013), and that BC AAOD data is only scarcely available in the Plateau and adjacent regions.

Another equally important factor contributing to the large discrepancy is the assumption of external mixing of BC in the model, which leads to weaker BC absorption (Jacobson, 2001). Previous studies have found that BC absorption is enhanced by 50 % due to internal mixing (Bond et al., 2006). A 50 % increase to our model results would largely reduce the discrepancy, particularly for sites in the Indo-Gangetic Plain and the southeastern Plateau and to the northeast of the Plateau (Table 3 and Fig. 9). There is evidence that the enhancement of BC absorption due to internal mixing may be considerably smaller than previously thought (Cappa et al., 2012). It is clear that the large discrepancy of more than a factor of two in the Himalayas and to the northwest of the Plateau cannot be fully explained by the lack of BC internal mixing consideration (and the associated larger absorption) in the model. Bond et al. (2013) pointed out that most models significantly underestimate BC AAOD, particularly in South and Southeast Asia, primarily because of the absence of internal mixing and the underestimated emissions. They recommended scaling up modeled BC AAOD to AEROENT observations in order to accurately estimate BC radiative effects.

Therefore, although surface BC concentration is relatively well captured by model results (see Sect. 3.1), more measurements of vertical profiles over the Tibetan Plateau are imperative for evaluating column quantities such as BC AAOD.

ACPD
14, 7305–7354, 2014

4 Sensitivity to BC emissions

Figure 3 shows that model simulated surface BC concentrations are considerably lower in experiment B (using the INTEX-B inventory) relative to experiment A (using the LU inventory). The difference in surface BC concentration is more than 30 % at rural sites and 10–20 % at remote sites, decreasing with distance from the source region. Such varying difference in surface BC concentration largely reflects the spatially non-uniform differences between the two emission inventories. The difference in BC concentration in snow between the two sets of results is less than 20 %. The relatively smaller difference is because the sites with measurements of BC concentration in snow are invariably remote high-elevation sites, further away from the source regions. BC concentrations in snow are higher over the northwestern and northeastern Plateau and to the north of the Plateau but lower in the Himalayas and the central Plateau in experiment B than in A. This is because of the lower BC emissions in the central Plateau and India and the higher emissions in northwestern and central China in the INTEX-B than in the LU inventories. BC AAOD values are higher (< 15 %) to the northeast and northwest of the Plateau and lower (10–60 %) in the Indo-Gangetic Plain in experiment B than in A. Therefore, both surface BC concentration and AAOD along the southern slope of the Himalayas are strongly sensitive to Indian emissions, while the high-altitude remote sites are less affected by the emission changes in the source regions. Overall, experiment B results show larger negative bias and root mean square error (RMSE) (Table 6) and lower Taylor score (Fig. 10) relative to experiment A. As such, our results suggest that the INTEX-B inventory considerably underestimates anthropogenic BC emissions in India.

5 Sensitivity to BC aging parameterization

Compared with model results from the standard simulation (experiment A, Table 5), the use of Liu et al. (2012) parameterization for BC aging in the model (experiment C, Ta-

ACPD
14, 7305–7354, 2014

ble 5) results in increased surface BC concentrations, BC concentrations in snow, and BC AAOD, because of the longer BC atmospheric lifetime against wet scavenging (see Sect. 2.2.3). The increase in surface BC concentration is 1 % on average (maximum 3 %) at rural sites and 10 % on average (maximum 30 %) at remote sites (Fig. 3). The increase in BC AAOD is 10 % on average (maximum 30 %) at most AERONET sites but leads to lower spatiotemporal correlations with observations (Table 6). The aging parameterization has a much stronger impact on model simulated BC concentration in snow than on surface BC concentration and BC AAOD. The increase in BC concentration in snow is more than 30 % at a number of sites in the Himalayas and the central Plateau (Table 2). Compared with the standard simulation (experiment A), the use of the Liu et al. (2012) parameterization results in an overestimate of BC concentration in snow relative to observations, which increases the absolute bias by a factor of two (Table 6) and decreases the Taylor score (Fig. 10). This suggests that the Liu et al. (2011) aging parameterization may result in too long conversion times of BC (from hydrophobic to hydrophilic) hence too long atmospheric lifetimes.

6 Summary and conclusions

We systematically evaluated global 3-D chemical transport model simulations of BC in the Tibetan Plateau against surface measurements of BC in surface air, BC in snow, and BC AAOD for 2006.

Model results captured the seasonal variation of surface BC concentrations, but the observed winter high values at rural sites were absent in the model. Model simulated surface BC concentrations at remote sites were generally within a factor of two of the observations. Model simulated BC concentrations in snow were spatiotemporally consistent with observations. Model results were too high at several sites in the Himalayas and too low in the central Tibetan Plateau. The highest concentrations of surface BC and BC in snow were seen north of the Plateau (40° N–50° N) and along the southern slope of the Himalayas during non-monsoon season. Model results of both surface BC

ACPD
14, 7305–7354, 2014

and BC in snow showed no statistically significant difference with observations with biases less than 15 %. Model results of BC AAOD were biased low at most AERONET sites over the Plateau, especially to the northwest of the Plateau and in the Himalayas during winter and spring. This large negative bias were mainly because of the underestimated emissions and the assumption of external mixing in the model, though the retrieved AAOD has a positive bias (Bond et al., 2013). This implies that the modeled BC AAOD probably should be scaled to AERONET observations in order to correctly estimate BC climate forcing.

Sensitivity tests showed that the emissions from China and India had a large impact on surface BC and AAOD simulations over the Tibetan Plateau, while the BC aging mainly affected simulations of BC in snow. Uncertainty analysis implied that model emissions, wet deposition and transport over the Himalayas were important sources of uncertainties. However, more quantitative analyses are required to investigate the relative contribution from each factor.

Acknowledgements. We thank Paolo Bonasoni, Angela Marinoni, Stefano Decesari, Krishnaswamy Krishnamoorthy, Suresh Babu, and Monika Kopacz for offering useful information. We thank James T. Randerson for providing biomass burning emissions with small fires. This study also used the data collected within the SHARE Project thanks to contributions from the Italian National Research Council and the Italian Ministry of Foreign Affairs. This study was funded by NASA grants NNX09AF07G and NNX08AF64G from the Atmospheric Chemistry Modeling and Analysis Program (ACMAP).

References

Allen, D. J., Rood, R. B., Thompson, A. M., and Hudson, R. D.: Three-dimensional radon 222 calculations using assimilated meteorological data and a convective mixing algorithm, J. Geophys. Res.-Atmos., 101, 6871–6881, doi:10.1029/95jd03408, 1996a.

Allen, D. J., Kasibhatla, P., Thompson, A. M., Rood, R. B., Doddridge, B. G., Pickering, K. E., Hudson, R. D., and Lin, S. J.: Transport-induced interannual variability of carbon monoxide

ACPD
14, 7305–7354, 2014

determined using a chemistry and transport model, J. Geophys. Res.-Atmos., 101, 28655–28669, doi:10.1029/96jd02984, 1996b.

Andermann, C., Bonnet, S., and Gloaguen, R.: Evaluation of precipitation data sets along the Himalayan front, Geochem. Geophy. Geosy., 12, Q07023, doi:10.1029/2011gc003513, 2011.

Arakawa, A. and Schubert, W. H.: Interaction of a Cumulus Cloud Ensemble with Large-Scale Environment 1., J. Atmos. Sci., 31, 674–701, doi:10.1175/1520-0469(1974)031<0674:IOACCE>2.0.CO;2, 1974.

Barnett, T. P., Adam, J. C., and Lettenmaier, D. P.: Potential impacts of a warming climate on water availability in snow-dominated regions, Nature, 438, 303–309, doi:10.1038/Nature04141, 2005.

Beegum, S. N., Moorthy, K. K., Babu, S. S., Satheesh, S. K., Vinoj, V., Badarinath, K. V. S., Safai, P. D., Devara, P. C. S., Singh, S., Vinod, Durnka, U. C., and Pant, P.: Spatial distribution of aerosol black carbon over India during pre-monsoon season, Atmos. Environ., 43, 1071–1078, doi:10.1016/j.atmosenv.2008.11.042, 2009.

Bey, I., Jacob, D. J., Yantosca, R. M., Logan, J. A., Field, B. D., Fiore, A. M., Li, Q. B., Liu, H. G. Y., Mickley, L. J., and Schultz, M. G.: Global modeling of tropospheric chemistry with assimilated meteorology: model description and evaluation, J. Geophys. Res., 106, 23073–23095, doi:10.1029/2001jd000807, 2001.

Bonasoni, P., Laj, P., Marinoni, A., Sprenger, M., Angelini, F., Arduini, J., Bonafè, U., Calzolari, F., Colombo, T., Decesari, S., Di Biagio, C., di Sarra, A. G., Evangelisti, F., Duchi, R., Facchini, MC., Fuzzi, S., Gobbi, G. P., Maione, M., Panday, A., Roccato, F., Sellegri, K., Venzac, H., Verza, GP., Villani, P., Vuillermoz, E., and Cristofanelli, P.: Atmospheric Brown Clouds in the Himalayas: first two years of continuous observations at the Nepal Climate Observatory-Pyramid (5079 m), Atmos. Chem. Phys., 10, 7515–7531, doi:10.5194/acp-10-7515-2010, 2010.

Bond, T. C., Anderson, T. L., and Campbell, D.: Calibration and intercomparison of filter-based measurements of visible light absorption by aerosols, Aerosol Sci. Tech., 30, 582–600, doi:10.1080/027868299304435, 1999.

Bond, T. C., Streets, D. G., Yarber, K. F., Nelson, S. M., Woo, J. H., and Klimont, Z.: A technology-based global inventory of black and organic carbon emissions from combustion, J. Geophys. Res., 109, D14203, doi:10.1029/2003jd003697, 2004.

ACPD
14, 7305–7354, 2014

Bond, T. C., Habib, G., and Bergstrom, R. W.: Limitations in the enhancement of visible light absorption due to mixing state, J. Geophys. Res.-Atmos., 111, D20211, doi:10.1029/2006jd007315, 2006.

Bond, T. C., Bhardwaj, E., Dong, R., Jogani, R., Jung, S. K., Roden, C., Streets, D. G., and Trautmann, N. M.: Historical emissions of black and organic carbon aerosol from energy-related combustion, 1850–2000, Global Biogeochem. Cy., 21, Gb2018, doi:10.1029/2006gb002840, 2007.

Bond, T. C., Doherty, S. J., Fahey, D. W., Forster, P. M., Berntsen, T., DeAngelo, B. J., Flanner, M. G., Ghan, S., Kärcher, B., Koch, D., Kinne, S., Kondo, Y., Quinn, P. K., Sarofim, M. C., Schultz, M. G., Schulz, M., Venkataraman, C., Zhang, H., Zhang, S., Bellouin, N., Guttikunda, S. K., Hopke, P. K., Jacobson, M. Z., Kaiser, J. W., Klimont, Z., Lohmann, U., Schwarz, J. P., Shindell, D., Storelvmo, T., Warren, S. G., and Zender, C. S.: Bounding the role of black carbon in the climate system: a scientific assessment, J. Geophys. Res.-Atmos., 118, 1–173, doi:10.1002/jgrd.50171, 2013.

Cachier, H. and Pertuisot, M. H.: Particulate carbon in Arctic ice, Analysis Magazine, 22, 34–37, 1994.

Carrico, C. M., Bergin, M. H., Shrestha, A. B., Dibb, J. E., Gomes, L., and Harris, J. M.: The importance of carbon and mineral dust to seasonal aerosol properties in the Nepal Himalaya, Atmos. Environ., 37, 2811–2824, doi:10.1016/S1352-2310(03)00197-3, 2003.

Cappa, C. D., Onasch, T. B., Massoli, P., Worsnop, D. R., Bates, T. S., Cross, E. S., Davidovits, P., Hakala, J., Hayden, K. L., Jobson, B. T., Kolesar, K. R., Lack, D. A., Lerner, B. M., Li, S. M., Mellon, D., Nuaaman, I., Olfert, J. S., Petaja, T., Quinn, P. K., Song, C., Subramanian, R., Williams, E. J., and Zaveri, R. A.: Radiative absorption enhancements due to the mixing state of atmospheric black carbon, Science, 337, 1078–1081, doi:10.1126/science.1223447, 2012.

Chen, D., Wang, Y., McElroy, M. B., He, K., Yantosca, R. M., and Le Sager, P.: Regional CO pollution and export in China simulated by the high-resolution nested-grid GEOS-Chem model, Atmos. Chem. Phys., 9, 3825–3839, doi:10.5194/acp-9-3825-2009, 2009.

Chow, J. C., Watson, J. G., Chen, L. W. A., Arnott, W. P., Moosmuller, H., and Fung, K.: Equivalence of elemental carbon by thermal/optical reflectance and transmittance with different temperature protocols, Environ. Sci. Technol., 38, 4414–4422, doi:10.1021/Es034936u, 2004.

Cooke, W. F., Liousse, C., Cachier, H., and Feichter, J.: Construction of a $1^{\circ} \times 1^{\circ}$ fossil fuel emission data set for carbonaceous aerosol and implementation and radiative impact in the

ACPD
14, 7305–7354, 2014

ECHAM4 model, J. Geophys. Res.-Atmos., 104, 22137–22162, doi:10.1029/1999jd900187, 1999.

Donner, L. J., Wyman, B. L., Hemler, R. S., Horowitz, L. W., Ming, Y., Zhao, M., Golaz, J. C., Ginoux, P., Lin, S. J., Schwarzkopf, M. D., Austin, J., Alaka, G., Cooke, W. F., Delworth, T. L., Freidenreich, S. M., Gordon, C. T., Griffies, S. M., Held, I. M., Hurlin, W. J., Klein, S. A., Knutson, T. R., Langenhorst, A. R., Lee, H. C., Lin, Y. L., Magi, B. I., Malyshev, S. L., Milly, P. C. D., Naik, V., Nath, M. J., Pincus, R., Ploshay, J. J., Ramaswamy, V., Seman, C. J., Shevliakova, E., Sirutis, J. J., Stern, W. F., Stouffer, R. J., Wilson, R. J., Winton, M., Wittenberg, A. T., and Zeng, F. R.: The Dynamical Core, physical parameterizations, and basic simulation characteristics of the atmospheric component AM3 of the GFDL Global Coupled Model CM3, J. Climate, 24, 3484–3519, doi:10.1175/2011jcli3955.1, 2011.

Dubovik, O. and King, M. D.: A flexible inversion algorithm for retrieval of aerosol optical properties from Sun and sky radiance measurements, J. Geophys. Res.-Atmos., 105, 20673–20696, doi:10.1029/2000jd900282, 2000.

Emery, C., Jung, J., Downey, N., Johnson, J., Jimenez, M., Yarvvood, G., and Morris, R.: Regional and global modeling estimates of policy relevant background ozone over the United States, Atmos. Environ., 47, 206–217, doi:10.1016/j.atmosenv.2011.11.012, 2012.

Fairlie, T. D., Jacob, D. J., and Park, R. J.: The impact of transpacific transport of mineral dust in the United States, Atmos. Environ., 41, 1251–1266, doi:10.1016/j.atmosenv.2006.09.048, 2007.

Flanner, M. G., Zender, C. S., Randerson, J. T., and Rasch, P. J.: Present-day climate forcing and response from black carbon in snow, J. Geophys. Res.-Atmos., 112, D11202, doi:10.1029/2006jd008003, 2007.

Flanner, M. G., Zender, C. S., Hess, P. G., Mahowald, N. M., Painter, T. H., Ramanathan, V., and Rasch, P. J.: Springtime warming and reduced snow cover from carbonaceous particles, Atmos. Chem. Phys., 9, 2481–2497, doi:10.5194/acp-9-2481-2009, 2009.

Friedman, B., Herich, H., Kammermann, L., Gross, D. S., Arneth, A., Holst, T., and Cziczo, D. J.: Subarctic atmospheric aerosol composition: 1. Ambient aerosol characterization, J. Geophys. Res.-Atmos., 114, D13203, doi:10.1029/2009jd011772, 2009.

Ganguly, D., Ginoux, P., Ramaswamy, V., Dubovik, O., Welton, J., Reid, E. A., and Holben, B. N.: Inferring the composition and concentration of aerosols by combining AERONET and MPLNET data: comparison with other measurements and utilization to evaluate GCM output, J. Geophys. Res.-Atmos., 114, D16203, doi:10.1029/2009jd011895, 2009a.

ACPD
14, 7305–7354, 2014

Ganguly, D., Ginoux, P., Ramaswamy, V., Winker, D. M., Holben, B. N., and Tripathi, S. N.: Retrieving the composition and concentration of aerosols over the Indo-Gangetic basin using CALIOP and AERONET data, Geophys. Res. Lett., 36, L13806, doi:10.1029/2009gl038315, 2009b.

Granier, C., Bessagnet, B., Bond, T., D'Angiola, A., van der Gon, H. D., Frost, G. J., Heil, A., Kaiser, J. W., Kinne, S., Klimont, Z., Kloster, S., Lamarque, J. F., Liousse, C., Masui, T., Meleux, F., Mieville, A., Ohara, T., Raut, J. C., Riahi, K., Schultz, M. G., Smith, S. J., Thompson, A., van Aardenne, J., van der Werf, G. R., and van Vuuren, D. P.: Evolution of anthropogenic and biomass burning emissions of air pollutants at global and regional scales during the 1980–2010 period, Climatic Change, 109, 163–190, doi:10.1007/s10584-011-0154-1, 2011.

Hack, J. J.: Parameterization of moist convection in the National Center for Atmospheric Research Community Climate Model (CCM2), J. Geophys. Res.-Atmos., 99, 5551–5568, doi:10.1029/93jd03478, 1994.

Hansen, J. and Nazarenko, L.: Soot climate forcing via snow and ice albedos, P. Natl. Acad. Sci. USA, 101, 423–428, doi:10.1073/pnas.2237157100, 2004.

Harris, I., Jones, P. D., Osborn, T. J., and Lister, D. H.: Updated high-resolution grids of monthly climatic observations – the CRU TS3.10 Dataset, Int. J. Climatol., 34, 623–642, doi:10.1002/joc.3711, 2014.

Holtslag, A. A. M. and Boville, B. A.: Local versus nonlocal boundary-layer diffusion in a Global Climate Model, J. Climate, 6, 1825–1842, doi:10.1175/1520-0442(1993)006<1825:Lvnbld>2.0.Co;2, 1993.

Huffman, G. J., Adler, R. F., Morrissey, M. M., Bolvin, D. T., Curtis, S., Joyce, R., McGavock, B., and Susskind, J.: Global precipitation at one-degree daily resolution from multisatellite observations, J. Hydrometeorol., 2, 36–50, doi:10.1175/1525-7541(2001)002<0036:Gpaodd>2.0.Co;2, 2001.

Immerzeel, W. W., van Beek, L. P. H., and Bierkens, M. F. P.: Climate change will affect the Asian Water Towers, Science, 328, 1382–1385, doi:10.1126/science.1183188, 2010.

Jacobson, M. Z.: Strong radiative heating due to the mixing state of black carbon in atmospheric aerosols, Nature, 409, 695–697, doi:10.1038/35055518, 2001.

Jacobson, M. Z.: Climate response of fossil fuel and biofuel soot, accounting for soot's feedback to snow and sea ice albedo and emissivity, J. Geophys. Res.-Atmos., 109, D21201, doi:10.1029/2004jd004945, 2004.

ACPD
14, 7305–7354, 2014

Jacobson, M. Z.: Effects of externally-through-internally-mixed soot inclusions within clouds and precipitation on global climate, J. Phys. Chem. A, 110, 6860–6873, doi:10.1021/Jp056391r, 2006.

Kaiser, J. W., Heil, A., Andreae, M. O., Benedetti, A., Chubarova, N., Jones, L., Morcrette, J.-J., Razinger, M., Schultz, M. G., Suttie, M., and van der Werf, G. R.: Biomass burning emissions estimated with a global fire assimilation system based on observed fire radiative power, Biogeosciences, 9, 527–554, doi:10.5194/bg-9-527-2012, 2012.

Khalizov, A. F., Zhang, R. Y., Zhang, D., Xue, H. X., Pagels, J., and McMurry, P. H.: Formation of highly hygroscopic soot aerosols upon internal mixing with sulfuric acid vapor, J. Geophys. Res.-Atmos., 114, D05208, doi:10.1029/2008jd010595, 2009.

Kitoh, A. and Kusunoki, S.: East Asian summer monsoon simulation by a 20 km mesh AGCM, Clim. Dynam., 31, 389–401, doi:10.1007/s00382-007-0285-2, 2008.

Koch, D., Schulz, M., Kinne, S., McNaughton, C., Spackman, J. R., Balkanski, Y., Bauer, S., Berntsen, T., Bond, T. C., Boucher, O., Chin, M., Clarke, A., De Luca, N., Dentener, F., Diehl, T., Dubovik, O., Easter, R., Fahey, D. W., Feichter, J., Fillmore, D., Freitag, S., Ghan, S., Ginoux, P., Gong, S., Horowitz, L., Iversen, T., Kirkevåg, A., Klimont, Z., Kondo, Y., Krol, M., Liu, X., Miller, R., Montanaro, V., Moteki, N., Myhre, G., Penner, J. E., Perlwitz, J., Pitari, G., Reddy, S., Sahu, L., Sakamoto, H., Schuster, G., Schwarz, J. P., Seland, Ø., Stier, P., Takegawa, N., Takemura, T., Textor, C., van Aardenne, J. A., and Zhao, Y.: Evaluation of black carbon estimations in global aerosol models, Atmos. Chem. Phys., 9, 9001–9026, doi:10.5194/acp-9-9001-2009, 2009.

Kopacz, M., Mauzerall, D. L., Wang, J., Leibensperger, E. M., Henze, D. K., and Singh, K.: Origin and radiative forcing of black carbon transported to the Himalayas and Tibetan Plateau, Atmos. Chem. Phys., 11, 2837–2852, doi:10.5194/acp-11-2837-2011, 2011.

Lamarque, J.-F., Bond, T. C., Eyring, V., Granier, C., Heil, A., Klimont, Z., Lee, D., Liousse, C., Mieville, A., Owen, B., Schultz, M. G., Shindell, D., Smith, S. J., Stehfest, E., Van Aardenne, J., Cooper, O. R., Kainuma, M., Mahowald, N., McConnell, J. R., Naik, V., Riahi, K., and van Vuuren, D. P.: Historical (1850–2000) gridded anthropogenic and biomass burning emissions of reactive gases and aerosols: methodology and application, Atmos. Chem. Phys., 10, 7017–7039, doi:10.5194/acp-10-7017-2010, 2010.

Lau, K. M. and Kim, K. M.: Observational relationships between aerosol and Asian monsoon rainfall, and circulation, Geophys. Res. Lett., 33, L21810, doi:10.1029/2006gl027546, 2006.

ACPD
14, 7305–7354, 2014

Lau, W. K. M., Kim, M. K., Kim, K. M., and Lee, W. S.: Enhanced surface warming and accelerated snow melt in the Himalayas and Tibetan Plateau induced by absorbing aerosols, Environ. Res. Lett., 5, 025204, doi:10.1088/1748-9326/5/2/025204, 2010.

Lin, J. T. and McElroy, M. B.: Impacts of boundary layer mixing on pollutant vertical profiles in the lower troposphere: implications to satellite remote sensing, Atmos. Environ., 44, 1726–1739, doi:10.1016/j.atmosenv.2010.02.009, 2010.

Lin, J. T., Youn, D., Liang, X. Z., and Wuebbles, D. J.: Global model simulation of summertime US ozone diurnal cycle and its sensitivity to PBL mixing, spatial resolution, and emissions, Atmos. Environ., 42, 8470–8483, doi:10.1016/j.atmosenv.2008.08.012, 2008.

Lin, S. J. and Rood, R. B.: Multidimensional flux-form semi-Lagrangian transport schemes, Mon. Weather Rev., 124, 2046–2070, doi:10.1175/1520-0493(1996)124<2046:Mffslt>2.0.Co;2, 1996.

Liu, H. Y., Jacob, D. J., Bey, I., and Yantosca, R. M.: Constraints from Pb-210 and Be-7 on wet deposition and transport in a global three-dimensional chemical tracer model driven by assimilated meteorological fields, J. Geophys. Res.-Atmos., 106, 12109–12128, doi:10.1029/2000jd900839, 2001.

Liu, J. F., Fan, S. M., Horowitz, L. W., and Levy, H.: Evaluation of factors controlling long-range transport of black carbon to the Arctic, J. Geophys. Res.-Atmos., 116, D04307, doi:10.1029/2010jd015145, 2011.

Louis, J. F.: Parametric model of vertical eddy fluxes in the atmosphere, Bound.-Lay. Meteorol., 17, 187–202, doi:10.1007/Bf00117978, 1979.

Lu, Z., Zhang, Q., and Streets, D. G.: Sulfur dioxide and primary carbonaceous aerosol emissions in China and India, 1996–2010, Atmos. Chem. Phys., 11, 9839–9864, doi:10.5194/acp-11-9839-2011, 2011.

Lu, Z. F., Streets, D. G., Zhang, Q., and Wang, S. W.: A novel back-trajectory analysis of the origin of black carbon transported to the Himalayas and Tibetan Plateau during 1996–2010, Geophys. Res. Lett., 39, L01809, doi:10.1029/2011gl049903, 2012.

Ma, L. J., Zhang, T., Frauenfeld, O. W., Ye, B. S., Yang, D. Q., and Qin, D. H.: Evaluation of precipitation from the ERA-40, NCEP-1, and NCEP-2 Reanalyses and CMAP-1, CMAP-2, and GPCP-2 with ground-based measurements in China, J. Geophys. Res.-Atmos., 114, D09105, doi:10.1029/2008jd011178, 2009.

ACPD
14, 7305–7354, 2014

Mao, Y. H., Li, Q. B., Zhang, L., Chen, Y., Randerson, J. T., Chen, D., and Liou, K. N.: Biomass burning contribution to black carbon in the Western United States Mountain Ranges, Atmos. Chem. Phys., 11, 11253–11266, doi:10.5194/acp-11-11253-2011, 2011.
McMeeking, G. R., Good, N., Petters, M. D., McFiggans, G., and Coe, H.: Influences on the fraction of hydrophobic and hydrophilic black carbon in the atmosphere, Atmos. Chem. Phys., 11, 5099–5112, doi:10.5194/acp-11-5099-2011, 2011.
Menon, S., Koch, D., Beig, G., Sahu, S., Fasullo, J., and Orlikowski, D.: Black carbon aerosols and the third polar ice cap, Atmos. Chem. Phys., 10, 4559–4571, doi:10.5194/acp-10-4559-2010, 2010.
Mikhailov, E. F., Vlasenko, S. S., Kramer, L., and Niessner, R.: Interaction of soot aerosol particles with water droplets: influence of surface hydrophilicity, J. Aerosol Sci., 32, 697–711, doi:10.1016/S0021-8502(00)00101-4, 2001.
Ming, J., Cachier, H., Xiao, C., Qin, D., Kang, S., Hou, S., and Xu, J.: Black carbon record based on a shallow Himalayan ice core and its climatic implications, Atmos. Chem. Phys., 8, 1343–1352, doi:10.5194/acp-8-1343-2008, 2008.
Ming, J., Xiao, C. D., Cachier, H., Qin, D. H., Qin, X., Li, Z. Q., and Pu, J. C.: Black Carbon (BC) in the snow of glaciers in west China and its potential effects on albedos, Atmos. Res., 92, 114–123, doi:10.1016/j.atmosres.2008.09.007, 2009a.
Ming, J., Xiao, C., Du, Z., and Flanner, M. G.,: Black carbon in snow/ice of west China and its radiave forcing, Adv. Climate Change Res., 5, 328–35, 2009b (in Chinese with English abstract).
Ming, J., Xiao, C. D., Sun, J. Y., Kang, S. C., and Bonasoni, P.: Carbonaceous particles in the atmosphere and precipitation of the Nam Co region, central Tibet, J. Environ. Sci.-China, 22, 1748–1756, doi:10.1016/S1001-0742(09)60315-6, 2010.
Ming, J., Du, Z. C., Xiao, C. D., Xu, X. B., and Zhang, D. Q.: Darkening of the mid-Himalaya glaciers since 2000 and the potential causes, Environ. Res. Lett., 7, 014021, doi:10.1088/1748-9326/7/1/014021, 2012.
Ming, J., Xiao, C. D., Du, Z. C., and Yang, X. G.: An overview of black carbon deposition in High Asia glaciers and its impacts on radiation balance, Adv. Water Resour., 55, 80–87, doi:10.1016/j.advwatres.2012.05.015, 2013.
Moorthi, S. and Suarez, M. J.: Relaxed Arakawa–Schubert – a parameterization of moist convection for general-circulation models, Mon. Weather Rev., 120, 978–1002, doi:10.1175/1520-0493(1992)120<0978:Rasapo>2.0.Co;2, 1992.

ACPD
14, 7305–7354, 2014

Moorthy, K. K., Beegum, S. N., Srivastava, N., Satheesh, S. K., Chin, M., Blond, N., Babu, S. S., and Singh, S.: Performance evaluation of chemistry transport models over India, Atmos. Environ., 71, 210–225, 2013.

Nair, V. S., Moorthy, K. K., Alappattu, D. P., Kunhikrishnan, P. K., George, S., Nair, P. R., Babu, S. S., Abish, B., Satheesh, S. K., Tripathi, S. N., Niranjan, K., Madhavan, B. L., Srikant, V., Dutt, C. B. S., Badarinath, K. V. S., and Reddy, R. R.: Wintertime aerosol characteristics over the Indo-Gangetic Plain (IGP): impacts of local boundary layer processes and long-range transport, J. Geophys. Res.-Atmos., 112, D13205, doi:10.1029/2006jd008099, 2007.

Nair, V. S., Solmon, F., Giorgi, F., Mariotti, L., Babu, S. S., and Moorthy, K. K.: Simulation of South Asian aerosols for regional climate studies, J. Geophys. Res.-Atmos., 117, D04209, doi:10.1029/2011JD016711, 2012.

Painter, T. H., Flanner, M. G., Kaser, G., Marzeion, B., VanCuren, R. A., and Abdalati, W.: End of the Little Ice Age in the Alps forced by industrial black carbon, P. Natl. Acad. Sci. USA, 110, 15216–15221, doi:10.1073/pnas.1302570110, 2013.

Park, R. J., Jacob, D. J., Chin, M., and Martin, R. V.: Sources of carbonaceous aerosols over the United States and implications for natural visibility, J. Geophys. Res.-Atmos., 108, 4355, doi:10.1029/2002jd003190, 2003.

Park, R. J., Jacob, D. J., Palmer, P. I., Clarke, A. D., Weber, R. J., Zondlo, M. A., Eisele, F. L., Bandy, A. R., Thornton, D. C., Sachse, G. W., and Bond, T. C.: Export efficiency of black carbon aerosol in continental outflow: global implications, J. Geophys. Res.-Atmos., 110, D11205, doi:10.1029/2004jd005432, 2005.

Park, R. J., Jacob, D. J., Kumar, N., and Yantosca, R. M.: Regional visibility statistics in the United States: natural and transboundary pollution influences, and implications for the Regional Haze Rule, Atmos. Environ., 40, 5405–5423, doi:10.1016/j.atmosenv.2006.04.059, 2006.

Pathak, B., Kalita, G., Bhuyan, K., Bhuyan, P. K., and Moorthy, K. K.: Aerosol temporal characteristics and its impact on shortwave radiative forcing at a location in the northeast of India, J. Geophys. Res.-Atmos., 115, D19204, doi:10.1029/2009jd013462, 2010.

Petzold, A. and Schonlinner, M.: Multi-angle absorption photometry – a new method for the measurement of aerosol light absorption and atmospheric black carbon, J. Aerosol Sci., 35, 421–441, doi:10.1016/j.jaerosci.2003.09.005, 2004.

ACPD
14, 7305–7354, 2014

Prasad, A. K., Yang, K.-H. S., El-Askary, H. M., and Kafatos, M.: Melting of major Glaciers in the western Himalayas: evidence of climatic changes from long term MSU derived tropospheric temperature trend (1979–2008), Ann. Geophys., 27, 4505–4519, doi:10.5194/angeo-27-4505-2009, 2009.

Qian, Y., Flanner, M. G., Leung, L. R., and Wang, W.: Sensitivity studies on the impacts of Tibetan Plateau snowpack pollution on the Asian hydrological cycle and monsoon climate, Atmos. Chem. Phys., 11, 1929–1948, doi:10.5194/acp-11-1929-2011, 2011.

Qin, D. H., Liu, S. Y., and Li, P. J.: Snow cover distribution, variability, and response to climate change in western China, J. Climate, 19, 1820–1833, 2006.

Qu, W. J., Zhang, X. Y., Arimoto, R., Wang, D., Wang, Y. Q., Yan, L. W., and Li, Y.: Chemical composition of the background aerosol at two sites in southwestern and northwestern China: potential influences of regional transport, Tellus B, 60, 657–673, doi:10.1111/j.1600-0889.2008.00342.x, 2008.

Ram, K., Sarin, M. M., and Hegde, P.: Long-term record of aerosol optical properties and chemical composition from a high-altitude site (Manora Peak) in Central Himalaya, Atmos. Chem. Phys., 10, 11791–11803, doi:10.5194/acp-10-11791-2010, 2010a.

Ram, K., Sarin, M. M., and Tripathi, S. N.: A 1 year record of carbonaceous aerosols from an urban site in the Indo-Gangetic Plain: characterization, sources, and temporal variability, J. Geophys. Res.-Atmos., 115, D24313, doi:10.1029/2010jd014188, 2010b.

Ramanathan, V. and Carmichael, G.: Global and regional climate changes due to black carbon, Nat. Geosci., 1, 221–227, doi:10.1038/Ngeo156, 2008.

Ramanathan, V., Chung, C., Kim, D., Bettge, T., Buja, L., Kiehl, J. T., Washington, W. M., Fu, Q., Sikka, D. R., and Wild, M.: Atmospheric brown clouds: impacts on South Asian climate and hydrological cycle, P. Natl. Acad. Sci. USA, 102, 5326–5333, doi:10.1073/pnas.0500656102, 2005.

Ramanathan, V., Ramana, M. V., Roberts, G., Kim, D., Corrigan, C., Chung, C., and Winker, D.: Warming trends in Asia amplified by brown cloud solar absorption, Nature, 448, 575–578, doi:10.1038/Nature06019, 2007.

Randerson, J. T., Chen, Y., van der Werf, G. R., Rogers, B. M., and Morton, D. C.: Global burned area and biomass burning emissions from small fires, J. Geophys. Res.-Biogeo., 117, G04012, doi:10.1029/2012jg002128, 2012.

ACPD
14, 7305–7354, 2014

Sato, M., Hansen, J., Koch, D., Lacis, A., Ruedy, R., Dubovik, O., Holben, B., Chin, M., and Novakov, T.: Global atmospheric black carbon inferred from AERONET, P. Natl. Acad. Sci. USA, 100, 6319–6324, doi:10.1073/pnas.0731897100, 2003.

Schmid, H., Laskus, L., Abraham, H. J., Baltensperger, U., Lavanchy, V., Bizjak, M., Burba, P., Cachier, H., Crow, D., Chow, J., Gnauk, T., Even, A., ten Brink, H. M., Giesen, K. P., Hitzenberger, R., Hueglin, C., Maenhaut, W., Pio, C., Carvalho, A., Putaud, J. P., Toom-Sauntry, D., and Puxbaum, H.: Results of the "carbon conference" international aerosol carbon round robin test stage I, Atmos. Environ., 35, 2111–2121, doi:10.1016/S1352-2310(00)00493-3, 2001.

Singh, H. B., Brune, W. H., Crawford, J. H., Flocke, F., and Jacob, D. J.: Chemistry and transport of pollution over the Gulf of Mexico and the Pacific: spring 2006 INTEX-B campaign overview and first results, Atmos. Chem. Phys., 9, 2301–2318, doi:10.5194/acp-9-2301-2009, 2009.

Streets, D. G., Bond, T. C., Carmichael, G. R., Fernandes, S. D., Fu, Q., He, D., Klimont, Z., Nelson, S. M., Tsai, N. Y., Wang, M. Q., Woo, J. H., and Yarber, K. F.: An inventory of gaseous and primary aerosol emissions in Asia in the year 2000, J. Geophys. Res.-Atmos., 108, 8809, doi:10.1029/2002jd003093, 2003.

Taylor, K. E.: Summarizing multiple aspects of model performance in a single diagram, J. Geophys. Res.-Atmos., 106, 7183–7192, doi:10.1029/2000jd900719, 2001.

Textor, C., Schulz, M., Guibert, S., Kinne, S., Balkanski, Y., Bauer, S., Berntsen, T., Berglen, T., Boucher, O., Chin, M., Dentener, F., Diehl, T., Easter, R., Feichter, H., Fillmore, D., Ghan, S., Ginoux, P., Gong, S., Grini, A., Hendricks, J., Horowitz, L., Huang, P., Isaksen, I., Iversen, I., Kloster, S., Koch, D., Kirkevåg, A., Kristjansson, J. E., Krol, M., Lauer, A., Lamarque, J. F., Liu, X., Montanaro, V., Myhre, G., Penner, J., Pitari, G., Reddy, S., Seland, Ø., Stier, P., Takemura, T., and Tie, X.: Analysis and quantification of the diversities of aerosol life cycles within AeroCom, Atmos. Chem. Phys., 6, 1777–1813, doi:10.5194/acp-6-1777-2006, 2006.

van der Werf, G. R., Randerson, J. T., Giglio, L., Collatz, G. J., Mu, M., Kasibhatla, P. S., Morton, D. C., DeFries, R. S., Jin, Y., and van Leeuwen, T. T.: Global fire emissions and the contribution of deforestation, savanna, forest, agricultural, and peat fires (1997–2009), Atmos. Chem. Phys., 10, 11707–11735, doi:10.5194/acp-10-11707-2010, 2010.

Voisin, N., Wood, A. W., and Lettenmaier, D. P.: Evaluation of precipitation products for global hydrological prediction, J. Hydrometeorol., 9, 388–407, doi:10.1175/2007jhm938.1, 2008.

ACPD
14, 7305–7354, 2014

Walcek, C. J., Brost, R. A., Chang, J. S., and Wesely, M. L.: SO_2, sulfate and HNO_3 deposition velocities computed using regional land-use and meteorological data, Atmos. Environ., 20, 949–964, doi:10.1016/0004-6981(86)90279-9, 1986.

Wang, Q., Jacob, D. J., Fisher, J. A., Mao, J., Leibensperger, E. M., Carouge, C. C., Le Sager, P., Kondo, Y., Jimenez, J. L., Cubison, M. J., and Doherty, S. J.: Sources of carbonaceous aerosols and deposited black carbon in the Arctic in winter-spring: implications for radiative forcing, Atmos. Chem. Phys., 11, 12453–12473, doi:10.5194/acp-11-12453-2011, 2011.

Wang, Q., Jacob, D. J., Spackman, J. R., Perring, A. E., Schwarz, J. P., Moteki, N., Marais, E. A., Ge, C., Wang, J., and Barrett, S. R. H.: Global budget and radiative forcing of black carbon aerosol: constraints from pole-to-pole (HIPPO) observations across the Pacific, J. Geophys. Res.-Atmos., 119, 195–206, doi:10.1002/2013jd020824, 2014.

Wang, R., Tao, S., Wang, W. T., Liu, J. F., Shen, H. Z., Shen, G. F., Wang, B., Liu, X. P., Li, W., Huang, Y., Zhang, Y. Y., Lu, Y., Chen, H., Chen, Y. C., Wang, C., Zhu, D., Wang, X. L., Li, B. G., Liu, W. X., and Ma, J. M.: Black Carbon Emissions in China from 1949 to 2050, Environ. Sci. Technol., 46, 7595–7603, doi:10.1021/Es3003684, 2012.

Wang, Y. H., Jacob, D. J., and Logan, J. A.: Global simulation of tropospheric O_3-NO_x-hydrocarbon chemistry: 1. Model formulation, J. Geophys. Res.-Atmos., 103, 10713–10725, doi:10.1029/98jd00158, 1998.

Weingartner, E., Saathoff, H., Schnaiter, M., Streit, N., Bitnar, B., and Baltensperger, U.: Absorption of light by soot particles: determination of the absorption coefficient by means of aethalometers, J. Aerosol Sci., 34, 1445–1463, doi:10.1016/S0021-8502(03)00359-8, 2003.

Wesely, M. L.: Parameterization of surface resistances to gaseous dry deposition in regional-scale numerical models, Atmos. Environ., 23, 1293–1304, doi:10.1016/0004-6981(89)90153-4, 1989.

Wu, Q. B. and Liu, Y. Z.: Ground temperature monitoring and its recent change in Qinghai-Tibet Plateau, Cold Reg. Sci. Technol., 38, 85–92, doi:10.1016/S0165-232x(03)00064-8, 2004.

Xie, P. P. and Arkin, P. A.: Global precipitation: a 17 year monthly analysis based on gauge observations, satellite estimates, and numerical model outputs, B. Am. Meteorol. Soc., 78, 2539–2558, doi:10.1175/1520-0477(1997)078<2539:Gpayma>2.0.Co;2, 1997.

Xie, P. P., Yatagai, A., Chen, M. Y., Hayasaka, T., Fukushima, Y., Liu, C. M., and Yang, S.: A Gauge-based analysis of daily precipitation over East Asia, J. Hydrometeorol., 8, 607–626, doi:10.1175/Jhm583.1, 2007.

ACPD
14, 7305–7354, 2014

Xu, B., Yao, T., Liu, X., and Wang, N.: Elemental and organic carbon measurements with a two-step heating-gas chromatography system in snow samples from the Tibetan plateau, Ann. Glaciol., 43, 257–262, doi:10.3189/172756406781812122, 2006.

Xu, B. Q., Cao, J. J., Hansen, J., Yao, T. D., Joswia, D. R., Wang, N. L., Wu, G. J., Wang, M., Zhao, H. B., Yang, W., Liu, X. Q., and He, J. Q.: Black soot and the survival of Tibetan glaciers, P. Natl. Acad. Sci. USA, 106, 22114–22118, doi:10.1073/pnas.0910444106, 2009.

Yasunari, T. J., Bonasoni, P., Laj, P., Fujita, K., Vuillermoz, E., Marinoni, A., Cristofanelli, P., Duchi, R., Tartari, G., and Lau, K.-M.: Estimated impact of black carbon deposition during pre-monsoon season from Nepal Climate Observatory – Pyramid data and snow albedo changes over Himalayan glaciers, Atmos. Chem. Phys., 10, 6603–6615, doi:10.5194/acp-10-6603-2010, 2010.

Zhang, Q., Streets, D. G., Carmichael, G. R., He, K. B., Huo, H., Kannari, A., Klimont, Z., Park, I. S., Reddy, S., Fu, J. S., Chen, D., Duan, L., Lei, Y., Wang, L. T., and Yao, Z. L.: Asian emissions in 2006 for the NASA INTEX-B mission, Atmos. Chem. Phys., 9, 5131–5153, doi:10.5194/acp-9-5131-2009, 2009.

Zhang, R. Y., Khalizov, A. F., Pagels, J., Zhang, D., Xue, H. X., and McMurry, P. H.: Variability in morphology, hygroscopicity, and optical properties of soot aerosols during atmospheric processing, P. Natl. Acad. Sci. USA, 105, 10291–10296, doi:10.1073/pnas.0804860105, 2008.

Zhang, X. Y., Wang, Y. Q., Zhang, X. C., Guo, W., and Gong, S. L.: Carbonaceous aerosol composition over various regions of China during 2006, J. Geophys. Res.-Atmos., 113, D14111, doi:10.1029/2007jd009525, 2008.

Zhao, T. B. and Fu, C. B.: Comparison of products from ERA-40, NCEP-2, and CRU with station data for summer precipitation over China, Adv. Atmos. Sci., 23, 593–604, doi:10.1007/s00376-006-0593-1, 2006.

Zhou, G., Yao, T., Kang, S., Pu, J., Tian, L., Yang, W.: Mass balance of the Zhadang glacier in the central Tibetan Plateau. J. Glaciol. Geocryol., 29, 360–365, 2007 (in Chinese with English abstract).

ACPD
14, 7305–7354, 2014

Table 1. Observed and simulated surface BC concentrations over the Tibetan Plateau (see also Fig. 1).

Region	Site	Lat. (° N)	Lon. (° E)	Elev. (m)	Time	Freq.	Technique[a]	Surface BC ($\mu g\,m^{-3}$)			
								Obs.[b]	Exp. A[c]	Exp. B[d]	Exp. C[e]
Urban	Delhi	28.6	77.2	260	2006	monthly	Aethalometer	13.5[1]	2.6	1.7	2.6
	Dibrugarh	27.3	94.6	111	2008–2009	monthly	Aethalometer	8.9[2]	0.8	0.5	0.9
	Lhasa	29.7	91.1	3663	2006	monthly	TOR	3.7[3]	0.1	0.1	0.1
	Dunhuang	40.2	94.7	1139	2006	monthly	TOR	4.1[3]	0.1	0.2	0.1
Rural	Kharagpur	22.5	87.5	28	2006	monthly	Aethalometer	5.5[4]	4.2	2.4	4.2
	Kanpur	26.4	80.3	142	2006	monthly	TOT	3.7[5]	3.1	2.2	3.1
	Gandhi College	25.9	84.1	158	2006	monthly	Retrieval	4.8[6]	4.6	3.2	4.6
Remote	Nagarkot	27.7	85.5	2150	1999–2000	seasonal	TOT	1.0[7]	0.8	0.7	0.8
	NCOP	28.0	86.8	5079	2006	monthly	MAAP	0.2[8]	0.1	0.1	0.1
	Manora Peak	29.4	79.5	1950	2006	monthly	TOT	1.1[9]	1.3	1.2	1.3
	NCOS	30.8	91.0	4730	2006	monthly	TOR	0.1[10]	0.1	0.1	0.1
	Langtang	28.1	85.6	3920	1999–2000	seasonal	TOT	0.4[7]	0.4	0.4	0.4
	Zhuzhang	28.0	99.7	3583	2004–2005	monthly	TOR	0.3[11]	0.3	0.3	0.4

[a] Thermal Optical Reflectance (TOR), Thermal Optical Transmittance (TOT), Multi-Angle Absorption Photometer (MAAP).
[b] Values are multi-month averages. References: [1] Beegum et al. (2009), [2] Pathak et al. (2010), [3] Zhang et al. (2008), [4] Nair et al. (2012), [5] Ram et al. (2010b), [6] Ganguly et al. (2009b), [7] Carrico et al. (2003), [8] Bonasoni et al. (2010), [9] Ram et al. (2010a), [10] Ming et al. (2010), [11] Qu et al. (2008).
[c] Values from experiment A (Table 5) for 2006. See text for more details.
[d] Values from experiment B (Table 5) for 2006. See text for more details.
[e] Values from experiment C (Table 5) for 2006. See text for more details.

ACPD
14, 7305–7354, 2014

Table 2. Observed and simulated BC concentrations in snow over the Tibetan Plateau (see also Fig. 1).

Region	Site	Lat. (°N)	Lon. (°E)	Elev. (km)	Time	BC in snow ($\mu g kg^{-1}$)			
						Obs.[a]	Exp. A[b]	Exp. B[c]	Exp. C[d]
The Himalayas	Zuoqiupu	29.21	96.92	5.50	monsoon 2006	7.9[2]	22.5	18.4	25.5
		29.21	96.92	5.60	non-monsoon 2006	15.9[2]	21.2	18.3	31.9
	Qiangyong	28.83	90.25	5.40	summer 2001	43.1[1]	66.1	49.7	63.7
	Noijin Kangsang	29.04	90.20	5.95	annual 2005	30.6[2]	39.5	34.6	52.3
	East Rongbuk	28.02	86.96	6.50	monsoon 2001	35.0[3]	26.4	22.7	29.2
		28.02	86.96	6.50	non-monsoon 2001	21.0[3]	32.8	31.1	59.4
		28.02	86.96	6.50	summer 2002	20.3[4]	26.5	22.8	28.9
		28.02	86.96	6.50	Oct 2004	18.0[4]	20.5	20.8	26.0
		28.02	86.96	6.50	Sep 2006	9.0[7]	26.0	22.4	30.0
		28.02	86.96	6.52	May 2007	41.8[6]	27.1	24.7	29.7
	Kangwure	28.47	85.82	6.00	summer 2001	21.8[1]	26.5	22.8	28.9
	Namunani	30.45	81.27	5.90	summer 2004	4.3[1]	24.8	21.2	26.6
Northwestern Tibetan Plateau	Mt. Muztagh	38.28	75.02	6.35	summer 2001	37.2[1]	31.0	36.6	31.9
		38.28	75.10	6.30	1999	26.6[1]	33.0	36.4	45.8
Northeastern Tibetan Plateau	Laohugou #12	39.43	96.56	5.05	Oct 2005	35.0[4]	54.4	60.0	60.3
	Qiyi	39.23	97.06	4.85	Jul 2005	22.0[4]	25.7	30.3	27.4
	July 1 glacier	39.23	97.75	4.60	summer 2001	52.6[1]	59.2	68.8	61.0
Central Tibetan Plateau	Meikuang	35.67	94.18	5.20	summer 2001	446[1]	24.4	24.8	27.2
		35.67	94.18	5.20	Nov 2005	81.0[5]	40.9	43.3	50.5
	Tanggula	33.11	92.09	5.80	2003	53.1[2]	16.1	14.5	25.6
	Dongkemadi	33.10	92.08	5.60	summer 2001	18.2[1]	19.6	17.7	22.1
		33.10	92.08	5.60	year 2005	36.0[7]	15.8	14.2	23.7
	La'nong	30.42	90.57	5.85	Jun 2005	67.0[4]	39.1	35.9	37.8
	Zhadang	30.47	90.50	5.80	Jul 2006	87.4[4]	27.9	21.7	30.3
North of the Plateau	Haxilegen River	43.73	84.46	3.76	Oct 2006	46.9[4]	36.1	37.9	36.7
	Urumqi Riverhead	43.10	86.82	4.05	Nov 2006	141[5]	131.9	155.2	118.4
	Miao'ergou #3	43.06	94.32	4.51	Aug 2005	111[4]	98.8	113.2	103.7

[a] References: [1]Xu et al. (2006), [2]Xu et al. (2009), [3]Ming et al. (2008), [4]Ming et al. (2009a), [5]Ming et al. (2009b), [6]Ming et al. (2012), [7]Ming et al. (2013).
[b] Values from experiment A (Table 5) for 2006. See text for more details.
[c] Values from experiment B (Table 5) for 2006. See text for more details.
[d] Values from experiment C (Table 5) for 2006. See text for more details.

ACPD
14, 7305–7354, 2014

Table 3. Observed and simulated annual mean BC AAOD at AERONET sites over the Tibetan Plateau (see also Fig. 1).

Region	Site	Lat. (° N)	Lon. (° E)	Alt. (m)	Time	BC AAOD		
						Obs.[a]	Model[b]	Ratio[c]
The Indo-Gangetic Plain	Lahore	31.54	74.33	270	2007 ~ 2012	0.0434	0.0162	2.7
	Kanpur	26.51	80.23	123	2006 ~ 2012	0.0426	0.0221	1.9
	Gandhi College	25.87	84.13	60	2006 ~ 2012	0.0443	0.0282	1.6
	Gual_Pahari	28.43	77.15	384	2008 ~ 2010	0.0511	0.0222	2.3
	Jaipur	26.91	75.81	450	2009 ~ 2012	0.0202	0.0168	1.2
The Himalayas	Jomsom	28.78	83.71	2803	2012	0.0231	0.0136	1.7
	Pantnagar	29.05	79.52	241	2008 ~ 2009	0.0507	0.0114	4.4
	Nainital	29.36	79.46	1939	2008 ~ 2010	0.0204	0.0125	1.6
	Pokhara	28.15	83.97	807	2010 ~ 2012	0.0524	0.0056	9.4
	Kathmandu Univ.	27.60	85.54	1510	2009 ~ 2010	0.0406	0.0057	7.1
Northeastern Tibetan Plateau	SACOL	35.95	104.14	1965	2007 ~ 2011	0.0163	0.0100	1.6
Northeast of the Tibetan Plateau	Dalanzadgad	43.58	104.42	1470	2006, 2012	0.0038	0.0025	1.5
Northwest of the Tibetan Plateau	Issyk-Kul	42.62	76.98	1650	2008 ~ 2010	0.0196	0.0020	9.8
	Dushanbe	38.55	68.86	821	2011 ~ 2012	0.0131	0.0030	4.4

[a] AERONET retrieved BC AAOD (Bond et al., 2013). Values are multi-year averages.
[b] Values from experiment A (Table 5) for 2006. See text for more details.
[c] The ratio of AERONET retrieved to GEOS-Chem modeled BC AAOD.

ACPD
14, 7305–7354, 2014

Table 4. Anthropogenic BC emissions in China and India in 2006.

	China		India	
Emissions ($Gg\,yr^{-1}$)	Lu et al. (2011)	Zhang et al. (2009)	Lu et al. (2011)	Zhang et al. (2009)
Industry	509	575	201	47
Power plants	15	36	1	8
Residential	971	1022	608	268
Transportation	178	205	75	80
Total	1673 (954–3229*)	1838 (884–3823)	885 (522–1655)	404 (112–1454)

* Uncertainties (in parentheses).

ACPD
14, 7305–7354, 2014

Table 5. GEOS-Chem simulations of BC.

Model experiment		A	B	C
Anthropogenic emissions	China & India	Lu et al. (2011)	Zhang et al. (2009)	Lu et al. (2011)
	Rest of Asia		Zhang et al. (2009)	
	Rest of world		Bond et al. (2007)	
Biomass burning emissions		GFEDv3 (van der Werf et al., 2010), with updates from Randerson et al. (2012)		
BC aging (hydrophobic to hydrophilic)		e-folding time 1.15 days	e-folding time 1.15 days	Liu et al. (2011)
Deposition	Dry deposition	Wesely (1989) as implemented by Wang et al. (1998)		
	Wet deposition	Liu et al. (2001) with updates from Wang et al. (2011)		

ACPD
14, 7305–7354, 2014

Table 6. Error statistics of GEOS-Chem simulations of BC in the Tibetan Plateau for 2006.

Statistical quantities	BC in surface air			BC in snow			BC AAOD		
	Model experiments (see Table 5)								
	A	B	C	A	B	C	A	B	C
Mean Error	−0.29	−0.82	−0.26	−1.23	−0.75	3.39	−0.019	−0.023	−0.020
Mean Absolute Error	0.59	0.93	0.59	13.39	12.74	16.09	0.020	0.023	0.020
Fractional Gross Error	0.39	0.46	0.39	0.43	0.40	0.48	0.78	0.93	0.80
Root Mean Square Error (RMSE)	1.34	1.95	1.33	16.73	16.65	18.67	0.026	0.029	0.027
Bias-corrected RMSE	1.31	1.77	1.30	16.69	16.63	18.36	0.017	0.018	0.018
Correlation coefficient (p value < 0.001)	0.90	0.87	0.90	0.85	0.86	0.81	0.53	0.46	0.45

ACPD
14, 7305–7354, 2014

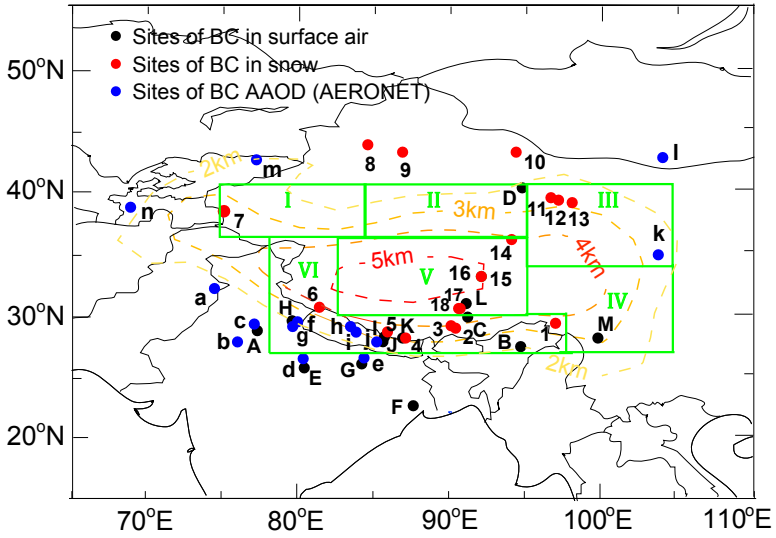

Fig. 1. BC measurements at sites in and around the Tibetan Plateau (see also Tables 1–3). Black circles are surface measurements: Delhi (A), Dibragarh (B), Lhasa (C), Dunhuang (D), Kanpur (E), Kharagpur (F), Gandhi College (G), Manora Peak (H), Langtang (I), Nagarkot (J), Nepal Climate Observatory at Pyramid (NCOP, K), Nam Co Observational Station (NCOS, L), Zhuzhang (M). Red circles are measurements of BC in snow: Zuoqiupu (1), Qiangyong (2), Noijin Kangsang (3), East Rongbuk (4), Kangwure (5), Namunani (6), Mt. Muztagh (7), Haxilegen Riverhead (8), Urumqi Riverhead (9), Miao'ergou No. 3 (10), Laohugou No. 12 (11), Qiyi (12), 1 July glacier (13), Meikuang (14), Tanggula (15), Dongkemadi (16), La'nong (17), Zhadang (18). Blue circles are BC AAOD measurements: Lahore (a), Jaipur (b), Gual_Pahari (c), Kanpur (d), Gandi college (e), Nainital (f), Pantnagar (g), Jomsom (h), Pokhara (i), Kathmandu University (j), SACOL (k), Dalanzadgad (l), Issyk-Kul (m), Dushanbe (n). The rectangles are the six sub-regions: the northwestern Plateau (I), the northern Plateau (II), the northeastern Plateau (III), the southeastern Plateau (IV), the central Plateau (V), and the Himalayas (VI). Topography is also shown (dashed colored contours).

ACPD
14, 7305–7354, 2014

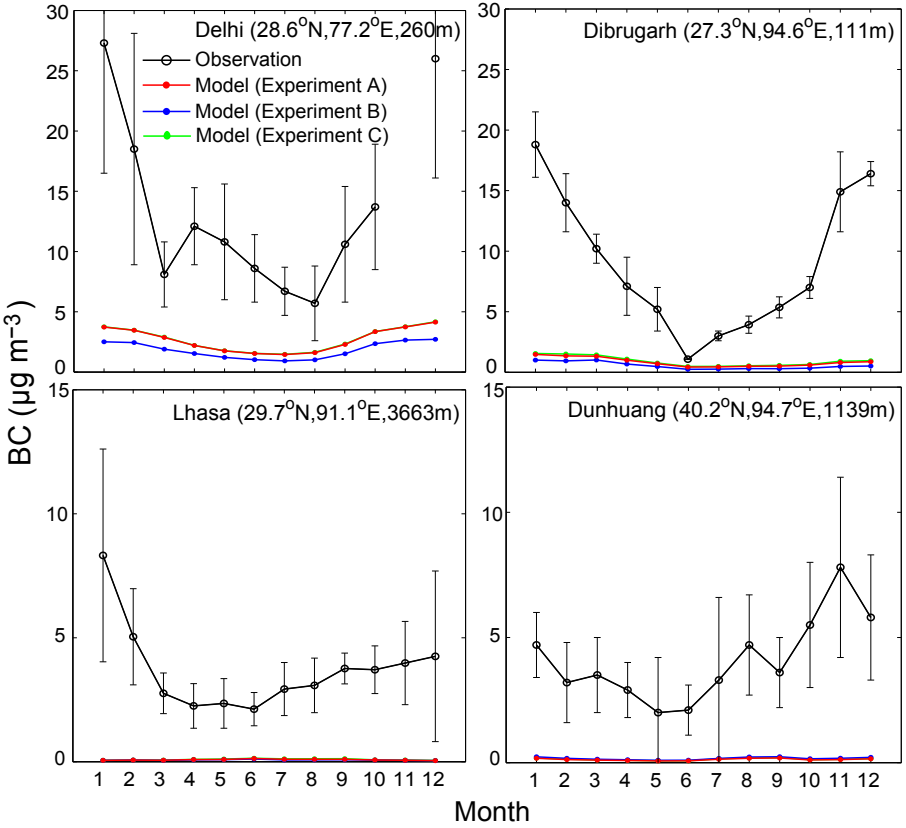

Fig. 2. Observed (black curve) and GEOS-Chem simulated (colored curves: red – experiment A; blue – experiment B; green – experiment C) monthly mean surface BC concentration ($\mu g\,m^{-3}$) at four urban sites around the Tibetan Plateau in 2006 (Table 1 and Fig. 1). Also shown are standard deviations for observations (error bars). See text for more details.

ACPD
14, 7305–7354, 2014

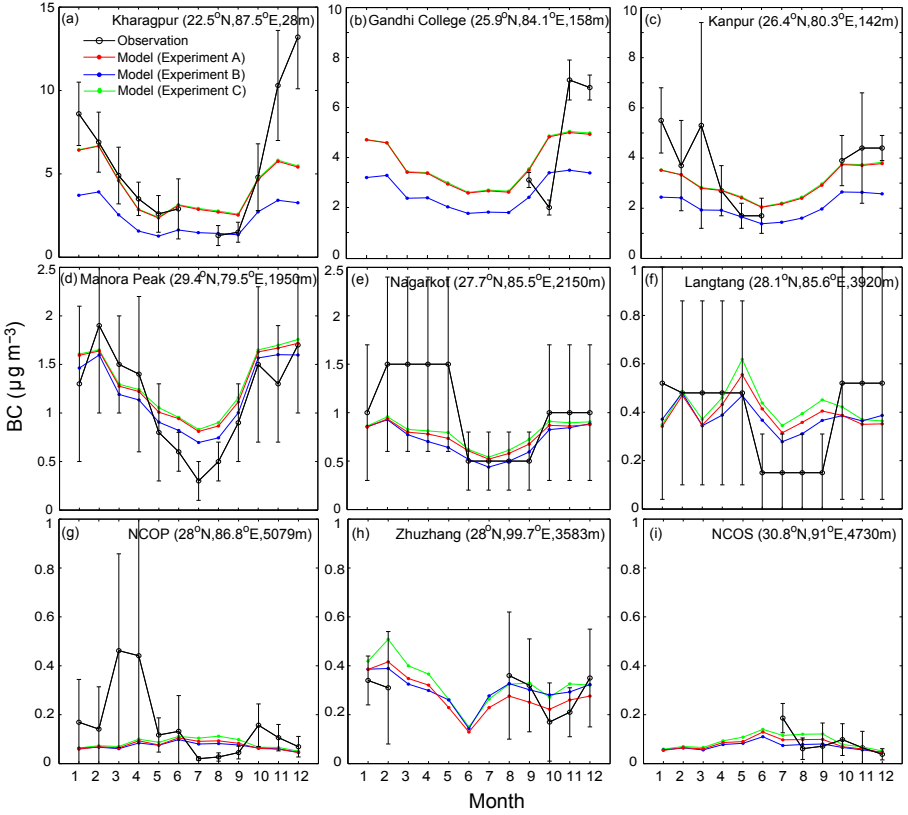

Fig. 3. Same as Fig. 2, but for three rural sites **(a–c)** and six remote sites **(d–i)** (see Table 1 and Fig. 1). Only seasonal mean observations are available at sites **(e)** and **(f)**.

ACPD
14, 7305–7354, 2014

A global 3-D CTM evaluation of black carbon in the Tibetan Plateau

C. He et al.

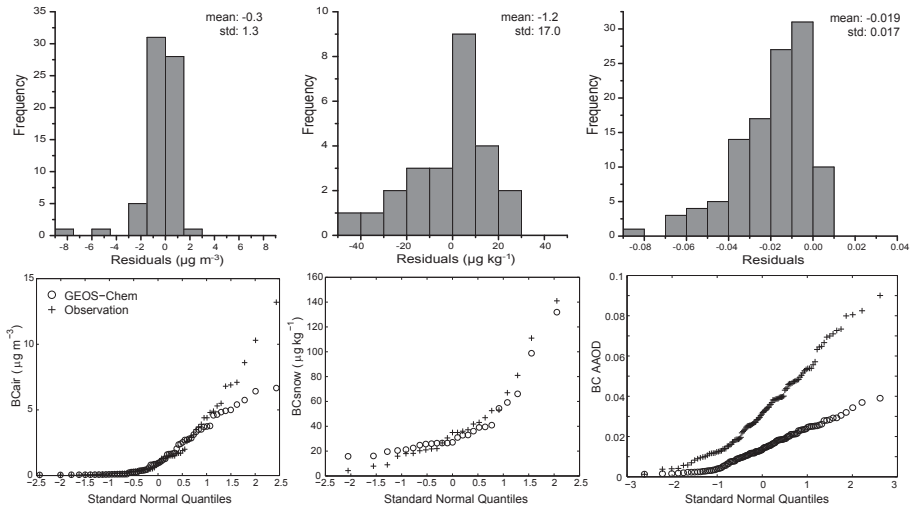

Fig. 4. Frequency histogram of residual errors (model – observation) (top row) and cumulative probability distributions (bottom row) for surface BC (left column), BC in snow (middle column), and BC AAOD (right column) at sites in and around the Tibetan Plateau (see Tables 1–3 and Fig. 1). Also shown are the mean and standard deviation of residual errors. Values are for 2006 unless stated otherwise. See text for details.

ACPD
14, 7305–7354, 2014

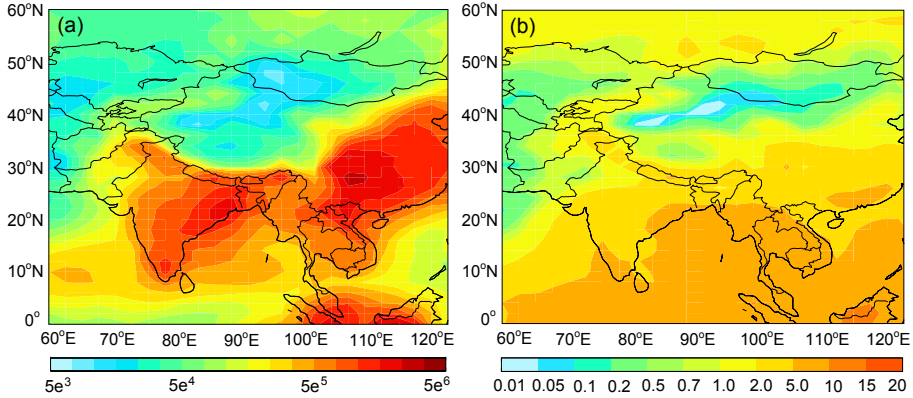

Fig. 5. (a) GEOS-Chem simulated annual mean total BC deposition (kg month^{-1}) over Asia and **(b)** GEOS-5 annual mean total precipitation (mm day^{-1}) over Asia. Values are for 2006.

ACPD
14, 7305–7354, 2014

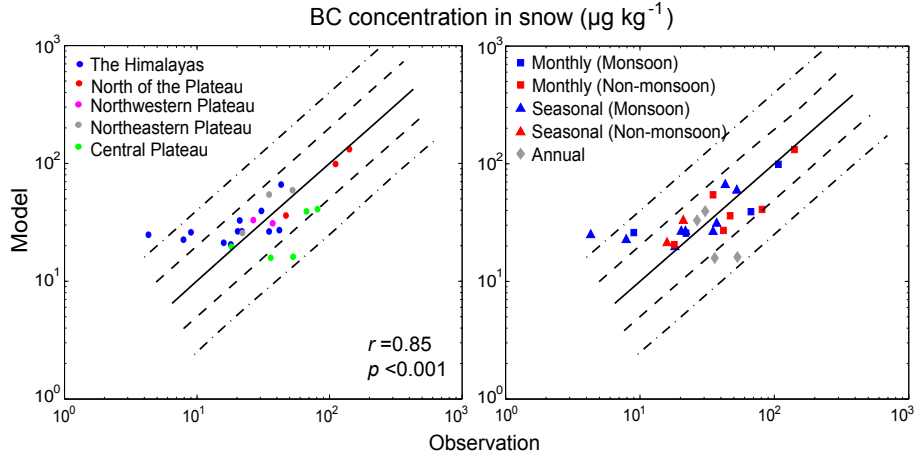

Fig. 6. Observed and GEOS-Chem simulated monthly or seasonal mean BC concentration in snow (μg kg^{-1}) at sites over the Tibetan Plateau (see Table 2 and Fig. 1). Left panel: sub-regions of the Tibetan Plateau are color coded. Right panel: different temporal resolutions are symbol-coded: monthly – square; seasonal – triangle; annual – diamond, with blue for monsoon season and red for non-monsoon season. Solid lines are 1 : 1 ratio lines; dashed lines are 1 : 2 (or 2 : 1) ratio lines; dashed-dotted lines are 1 : 4 (or 4 : 1) ratio lines. Also shown are the correlation coefficient (r) and p value. Values are for 2006 unless stated otherwise. See text for details.

ACPD
14, 7305–7354, 2014

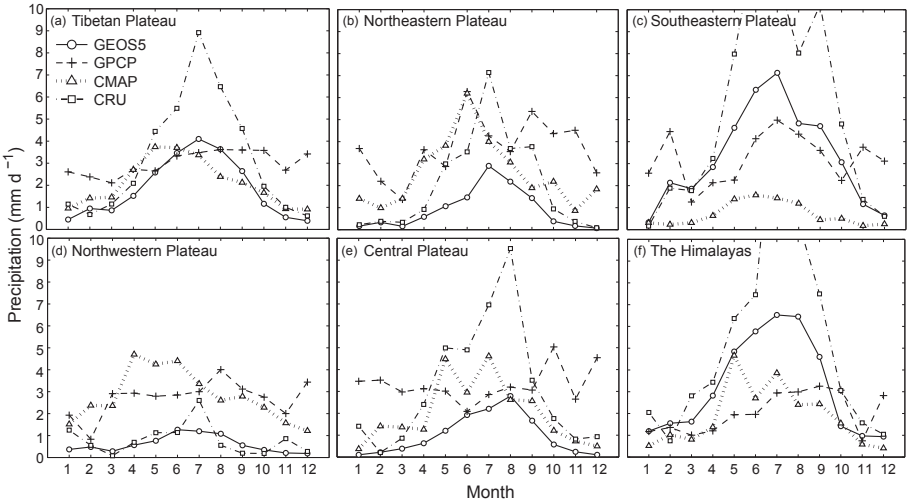

Fig. 7. Monthly mean precipitation (mm d^{-1}) in 2006, averaged over different parts of the Tibetan Plateau (see Fig. 1). Data is from the Goddard Earth Observing System Model version 5 (GEOS-5), Global Precipitation Climatology Project (GPCP), NOAA Climate Prediction Center (CPC) Merged Analysis of Precipitation (CMAP), and Climate Research Unit (CRU) of University of East Anglia.

ACPD
14, 7305–7354, 2014

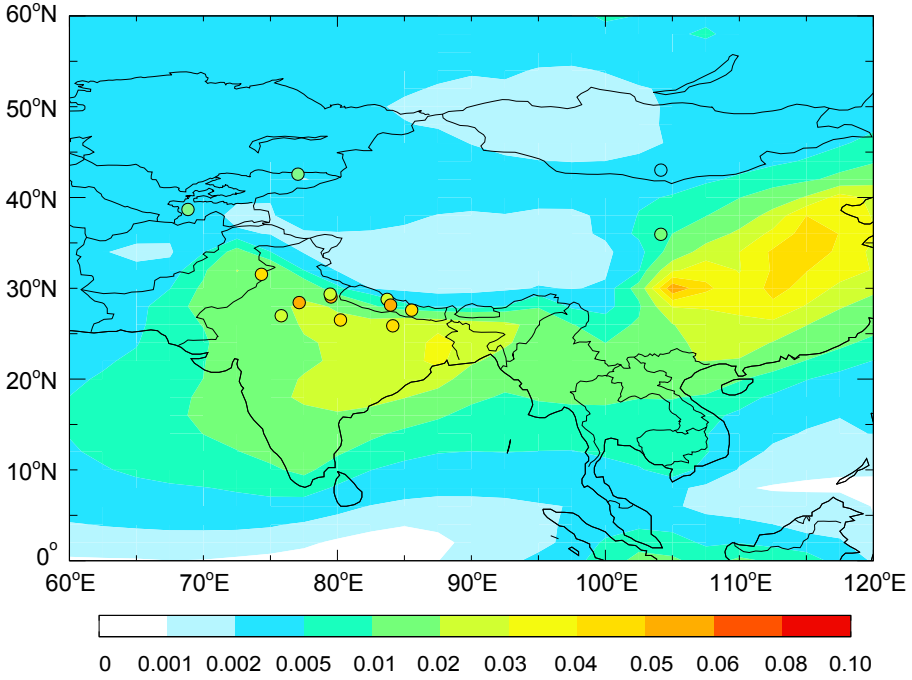

Fig. 8. GEOS-Chem simulated annual mean BC AAOD (color contours) for 2006. Colored circles are values retrieved from AERONET observations (see Table 3).

ACPD
14, 7305–7354, 2014

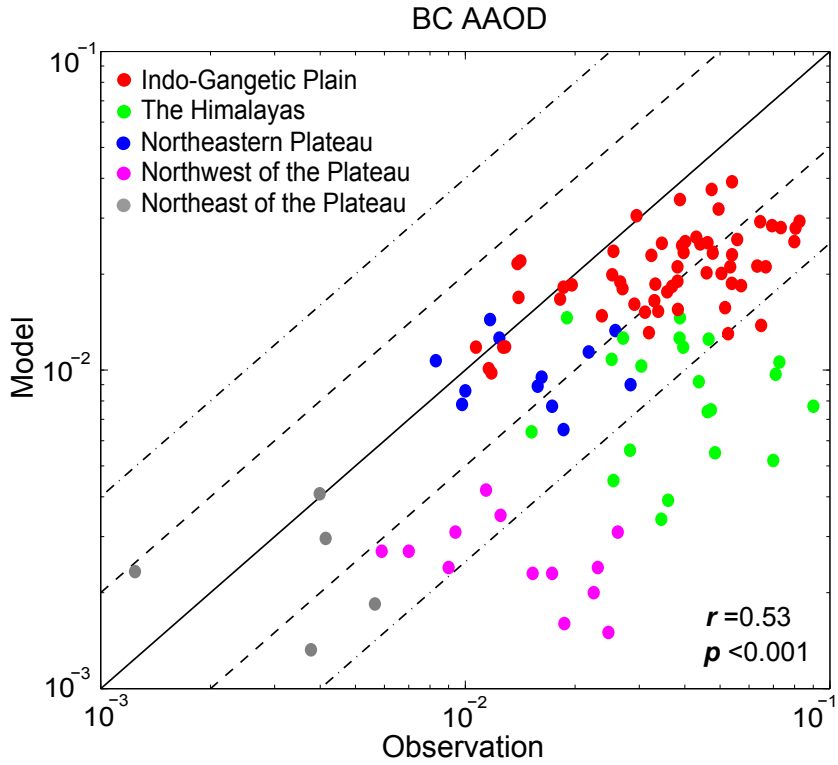

Fig. 9. Observed and GEOS-Chem simulated monthly mean BC AAOD at AERONET sites over the Tibetan Plateau (see Table 3 and Fig. 1). Different regions are color-coded: Indo-Gangetic Plain (red), the Himalayas (green), the northeastern Plateau (blue), Northeast of the Plateau (grey), Northwest of the Plateau (magenta). Solid line is 1 : 1 ratio line; dashed lines are 1 : 2 (or 2 : 1) ratio lines; dashed-dotted lines are 1 : 4 (or 4 : 1) ratio lines. Also shown are the correlation coefficient (r) and p value. Values are for 2006 unless stated otherwise. See text for details.

ACPD
14, 7305–7354, 2014

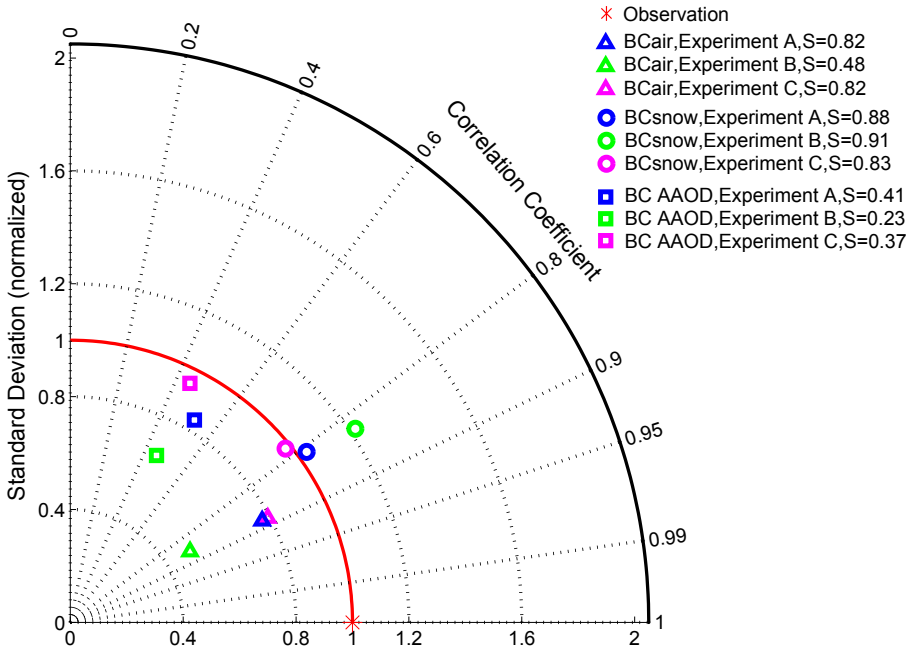

Fig. 10. Taylor diagram of GEOS-Chem simulated vs. observed BC concentration in surface air (BC_{air}) and in snow (BC_{snow}), and BC AAOD at sites over the Tibetan Plateau (see Tables 1–3 and Fig. 1). Red asterisk is the observation. Triangles, circles and squares, respectively, indicate modeled BC_{air}, BC_{snow}, and BC AAOD from experiments A (blue), B (green) and C (magenta). See Table 5 and text for more details on the model experiments. Also shown are the Taylor scores (S). Values are for 2006 unless stated otherwise. See text for details.

ACPD
14, 7305–7354, 2014